2016

3D Seismic Depth Imaging and Velocity Model Building in Anisotropic Media: Serri Oil and Gas Field, Saudi Arabia

Ali Jomaah Alsalem
University of South Carolina

3D Seismic Depth Imaging and Velocity Model Building in Anisotropic Media: Serri Oil and Gas Field, Saudi Arabia

by

Ali Jomaah Alsalem

Bachelor of Science
University of Durham, 2006

Submitted in Partial Fulfillment of the Requirements

For the Degree of Master of Science in

Geological Sciences

College of Arts and Sciences

University of South Carolina

2016

Accepted by:

Camelia Knapp, Director of Thesis

James Knapp, Reader

James Kellogg, Reader

Cheryl L. Addy, Vice Provost and Dean of the Graduate School

Acknowledgments

Firstly, my most sincere thanks to my thesis supervisor, Professor Camelia Knapp, for her unwavering support and guidance. Your passion for research is inspiring and your willingness to make time for me in your hectic schedule is greatly appreciated. I also wish to thank the other members of my thesis committee: Dr. James Knapp and Dr. James Kellogg for their support and friendship over the past two years.

Many thanks to Saudi Aramco for giving me this scholarship to be able to pursue my master in geological sciences and providing me with all the elegant financial support. Thanks for ETSD, my mother department, for working in providing me the dataset to carry out this research. Special thanks go to Michael Pittman from Saudi Aramco for his efforts to prepare the dataset and his advises on the seismic imaging. I would also like to thank Paradigm Company for their sate of art software, and particularly their support team for their continuous and always quick responses.

Reserved thanks to my parents overseas in Saudi Arabia. Thank you both for your love, prayers, support and guidance over the years. I would also like to thank my two beautiful daughters that make me forget all the exhaustion every time they welcome me at home with warm hugs. Finally, Special thanks are reserved for my wife Zahrah. You are my light and inspiration, always there when I need you with a smile. Your ceaseless love and support have made this possible, enjoyable and worthwhile.

Abstract

Seismic imaging is a significant element in hydrocarbon exploration to locate drilling prospects and it relies mainly on an accurate velocity model. Prestack depth migration (PreSDM) versus traditional post-stack time migration has become a common method for seismic velocity model building and imaging. This methodology accounts for seismic velocity anisotropy of the propagating waves in the subsurface with a higher level of accuracy in positioning the seismic events in their true positions in the subsurface.

In this thesis, we examine a 303 km^2 of 3D seismic data acquired by Saudi Aramco in the Serri field of North-West Saudi Arabia. The dataset is diagnosed to be of extremely poor reflective quality likely due to seismic anisotropic effects caused by shale deposits. Our main goal was to produce an enhanced and better focused seismic image that is geologically accurate and interpretable

This study develops a practical method for building an anisotropic velocity model to be further used in the anisotropic PreSDM. Based on this study, three main approaches have made a significant impact on the improvement of seismic imaging: (1) analysis of elastic reflection coefficients characterizing heterogeneities in the subsurface, (2) study of the variation of the reflection coefficients with the angle of incidence, and (3) a detailed characterization of the P-wave propagation velocity field. The seismic imaging results showed that PreSDM provided a significant improvement of the seismic image quality. Moreover, the anisotropic PreSDM provided more continuous and brighter reflections than the isotropic PreSDM.

Table of Contents

List of Figures

Chapter 1

Introduction

1.1 Introduction to Seismic Imaging

The reflection seismic method is based on sending elastic waves into the Earth and letting them propagate in all directions. In their travel to the subsurface, waves encounter heterogeneities, where they ‘refract’, ‘reflect’, or ‘convert’. The reflected energy travels back to the surface, where it is eventually measured by specific receivers and recorded. Seismic imaging have the objective to create from the recordings an image of these heterogeneities, which are mainly the geological features present in the subsurface. The geological heterogeneities in the subsurface are usually continuous laterally and therefore called layers or interfaces. These features are called ‘diffractors’ when they are more localized. In other words, refraction occurs wherever there is a change in propagation velocities and reflection takes place any time where the propagating wave encounters a change in velocity and density as we refer to as ‘acoustic impedance’ which is an elastic property of any medium. Consequently, the seismic image is an image of the ‘elastic reflectivity’ at each point of the subsurface. There are many types of seismic waves; and seismic reflection imaging deals mainly with primary waves (P-waves) which are compressional waves that are longitudinal in nature and travel through any type of material.

However, at elastic interfaces, part of the wave energy is converted into secondary waves (S-wave) which are shear waves that are transverse in nature and travel only through solids. (Robein, 2010)

Estimation of the velocity field of the Earth in which waves propagate is a key element to create an image of the subsurface. The amount of conversion depends on the 'angle of incidence' which is the angle measured from the normal to the interface. The reflection coefficient of the P-wave depends on this angle where the basic image depends on the reflectivity for a zero incidence angle. The reflection coefficient, in a mathematical sense, is derived from the logarithm of acoustic impedance. It is important to note that the elastic signal that is sent into the ground does not include all the frequencies which makes it bandlimited. Band-limitation happens because of the intrinsic physical limitations in sending very low frequencies in the ground and the normal attenuation of the high frequency components of waves as they propagate into Earth. Band-limitation affects the seismic image resolution. (Robein, 2010).

The seismic wave field is computed on a discrete grid in space and time. Migration methods are performed to compensate for refraction during the extrapolation of the wavefield in the subsurface. Unlike time migration (PSTM) where it assumes straight ray paths and corrects for refraction through a locally horizontal earth model, depth migration (PSDM) is done in a structural velocity in depth and it takes into account lateral variations in velocity within an earth model. Complex geology structures and changing in facies in the subsurface requires a significant attention to vertical and lateral variations in velocity. It is also as important to take into account that the subsurface is not homogeneous in nature, and rather anisotropic, which makes waves propagate at a velocity that depends on its

direction of propagation. It is therefore vital to account for the variation of the velocity, vertically and laterally, in order to construct the best model that can represent the Earth model.

Here, I use the 3D seismic data of the Serri oil field to perform a sequential velocity model building, the term ”velocity model building” in this thesis is used in a generalized sense to refer to the construction of a model. The velocity model building will aim to enhance the seismic image quality. So, in this introductory chapter, after I introduce the location of the Serri field, I will briefly discuss the major tectonic setting of the region and the geology of key formations of the study area. I will also describe how the data used in this thesis were acquired and pre-processed with preliminary analysis of the input gathers. The second chapter will give an introduction of the velocity model representation in a geological environment. There, I will show the initial stacking velocities (vertical functions) picking and creation of the CVS stack. The third chapter will feature the build-up of the isotropic model by firstly giving an introduction of the constrained velocity inversion (CVI) technique followed by the procedure and results. The fourth chapter in this thesis, will discuss the method used in depth migrating the seismic volume. There, I will provide an introduction to how the Kirchhoff wavefront PreSDM work. It will also display the results of migrating the data using the CVI isotropic model. The fifth chapter will be dedicated to the anisotropic velocity model building. I will first present the theory highlighting the VTI anisotropic type. Secondly, I will show the stages used to update the isotropic model using the depth gathers to create the anisotropic velocity model. In this chapter, a preSDM result from this model will be shown. The sixth chapter will contain a collective of images of preSDM results. There, I will compare and discuss the results from

the different stages of the seismic imaging presented in previous chapters. I will finally conclude this research by restating the importance of seismic imaging and giving recommendations to obtain better results.

1.2 Serri Field Location and Region Geological Settings

Figure 1.1 Serri Field Location map

The Serri field is, which part of the Arabia tectonic plate, located in the northern west region of Saudi Arabia and sits at some 40 km between the borders of Iraq and Jordan. Figure 1.1. This location attracts a deal of attention for hydrocarbon exploration of the area since the country targets more reserves in such undeveloped regions. Further in this section, I will briefly discuss the geological settings of the Arabian plate that led to the birth of this

field followed by stratigraphic geology enlightenment and how some of the formation were deposited.

The Arabian Plate is a minor tectonic plate in the northern and eastern hemispheres. It is one of three continental plates (the African, Arabian, and Indian Plates) that have been moving northward in recent geological history and colliding with the Eurasian Plate. There are 5 major tectonic settings in the geological history of the region (1) during the Precambrian Amar Collision (~640-530 Ma), the north-trending Precambrian Amar suture bisects the Arabian Peninsula creating a regional and regular north- trending structure pattern as result of compression (Ziegler, 2001). A basement depth map in figure 1.2 shows the adjacent structures in the North and Central Saudi Arabia with north-, north-east and north-west trending patterns including the greater Ghawar structure, Khurais, and Qatar dome. The North-South trending anticlines persisted elevated as horsts bounded by faults after the widespread extensional collapse of the Arabian shield that followed the Amar collision between 620 and 530 Ma. (2) The Late Devonian Hercynian Orogeny (~370-300 Ma): The Hercynian orogeny had a significant impact on the entire Arabian Plate. Multiple compressional phases affected the Arabian Peninsula during this period. Those compressional phases produced significant changes in the Arabian basin geometry. Uplifts, folding and inversion were also caused by those compressional events in the region. Many of the Hercynian faults bounding the major N-S uplifts were reactivated during the Triassic and late Cretaceous as discussed below. (3) The Early Triassic Zagros Rifting and Opening of Neo-Tethys Sea (260-240 Ma): During the Early Triassic, thermal subsidence and stretching of the Arabian plate due to the fragmenting of the Arabian-Gondwana\Iranian-Laurasia created widespread extensional faulting system. Zagros rifting caused the opening

of the Neo-Tethys Sea as shown in figure 1.3. Earlier Hercynian structures were reactivated and enhanced. (4) In the Late Cretaceous 1st Alpine Orogeny (~100 – 80 Ma), Alpine Orogeny began in the late Cretaceous through a compressional phase that caused the onset of closing the Neo-Tethys Sea affecting the Hercynian structures created in the region (Ziegler, 2001). (5) In the Second Alpine Orogeny (~35-20 Ma), the second episode of the Alpine Orogeny started in the middle to late Tertiary. It was associated with the opening of the Red Sea and collision of Arabia and Eurasia (Konert et al., 2001). Zagros orogeny was initiated from this collision of the Arabian plate and the Asia. The Arabian plate converged and subducted beneath Iran and caused the Arabian plate to tilt slightly to the northwest to form a series of anticlines and synclines in the Zagros Mountains (Konert et al., 2001)

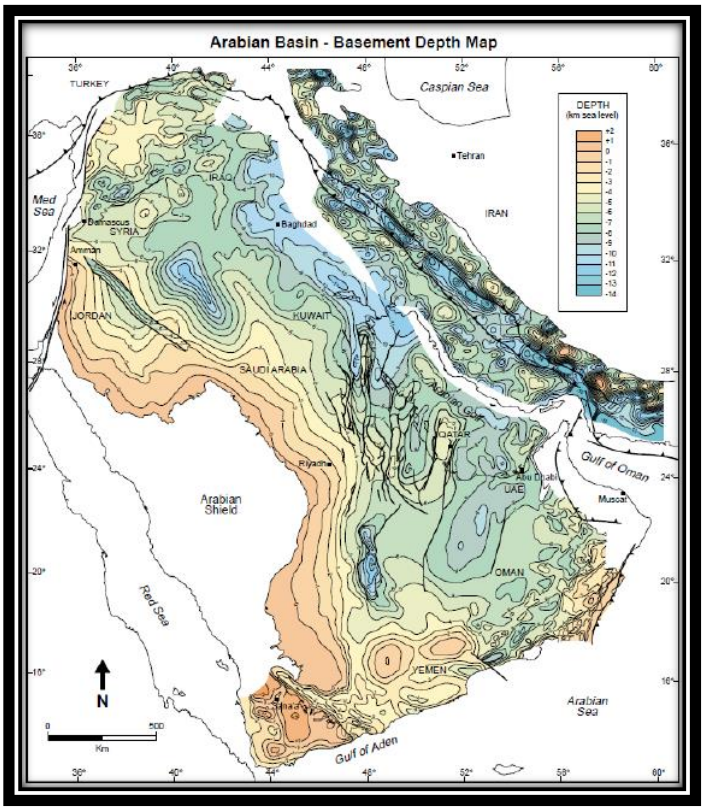

Figure 1.2. Crystalline Basement Isodepth Map from Ziegler (2001).

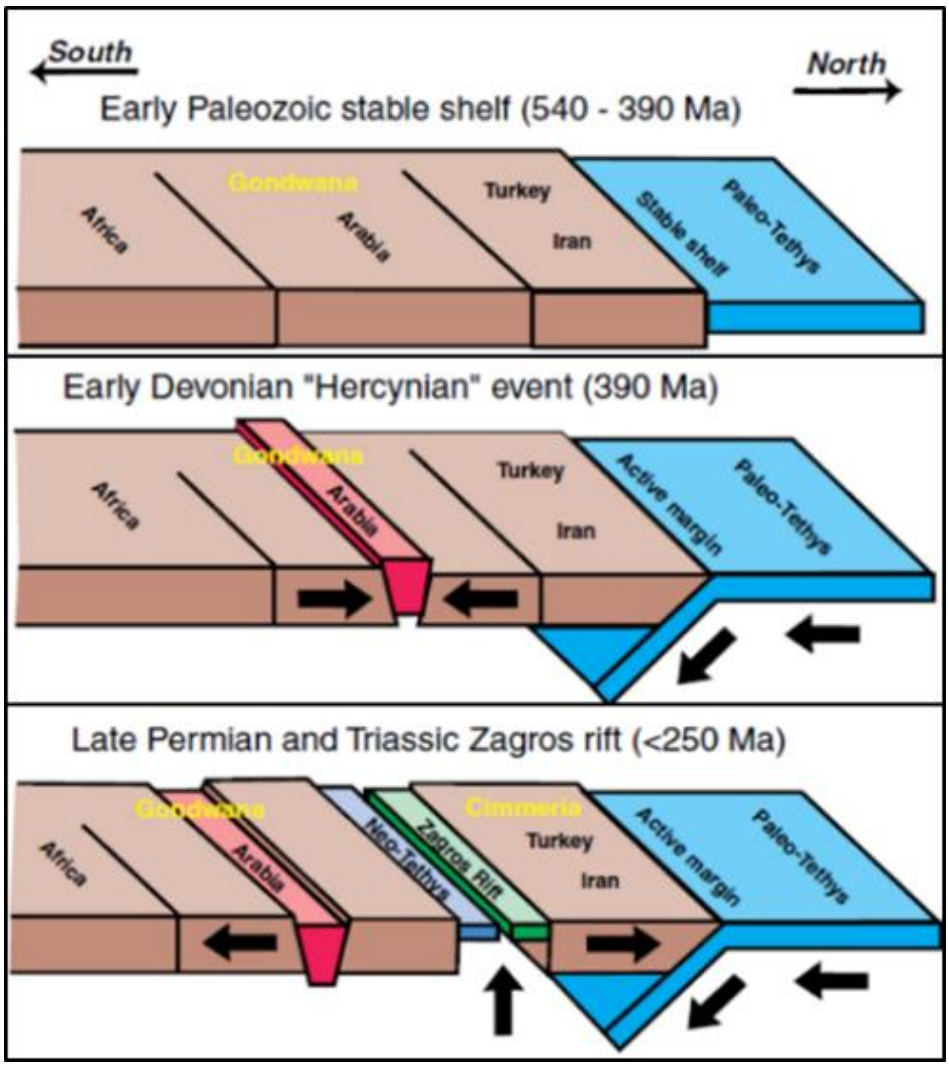

Figure 1.3 Schematic geological model of major tectonic events affecting the Arabian Plate Modified from McGilivray and Husseini (1992)

1.3 Stratigraphic Settings of Serri Field

Interests in the exploration for gas reserves in the North Western area in Saudi Arabia has always been a demand due the increased industrialization and power demand of the area. In this chapter, I will discuss the stratigraphic deposition of the main reservoir targets in the region (Figure 1.4). The Qasim formation was deposited in Middle to Upper Ordovician, consisting of four units: Hanadir, Kahfah, Ra'an and Quwara. The lowermost unit, Hanadir, is between 13 to 18 m in thickness and composed of shales deposited in a

shallow marine environment. Kahfah makes the thickest in this formation with 100 – 120 m of sandstone thickness in a shore-face environment. Ra'an unit was deposited in a calm marine setting and is composed of 30-36 m of silty clay. The uppermost unit, the Quwara, is a deep water open shelf consisting of shale. Zarga and Sarah formation were deposited during the glaciation toward the end of the Ordovician time forming channels of sandstones of maximum thickness of 100 m for Zarga and thicknesses of 83 m to 290 m for Sarah formation. Both formations frequently appear in the North Western section of Saudi Arabia and represent potential gas reservoir targets. The clastic Qalibah group was deposited in the Silurian and represents a regional regressive sequence. The Qalibah consists of two units: Qusaiba and Sharawra formations. Qusaiba formation is subdivided into five units representing cycles of transgressions and regressions in a lower to upper offshore domain forming stacked sedimentary sequences mainly composed of clayey siltstone. The shales in the base of Qusaiba formation represent a proven hydrocarbon source for the area. In some regions, during the deposition of the Qusaiba formation, there were igneous extrusion from subaerial volcanoes (Mahmoud et al, 1992). Sharwara formation is composed of siltstones and sandstones forming thicknesses between 315 to 430 m deposited in environments that vary from shallow to deep subtidal on a storm dominated shelf. (Saudi Stratigraphic Committee, 2013).

1.4 Available Dataset and Survey Design

Saudi Aramco Oil Company has thankfully provided the 3D seismic dataset that will be used in order to examine the processing techniques in this thesis. The 3D seismic data have been selected carefully and is known to have evident anisotropic effect from what

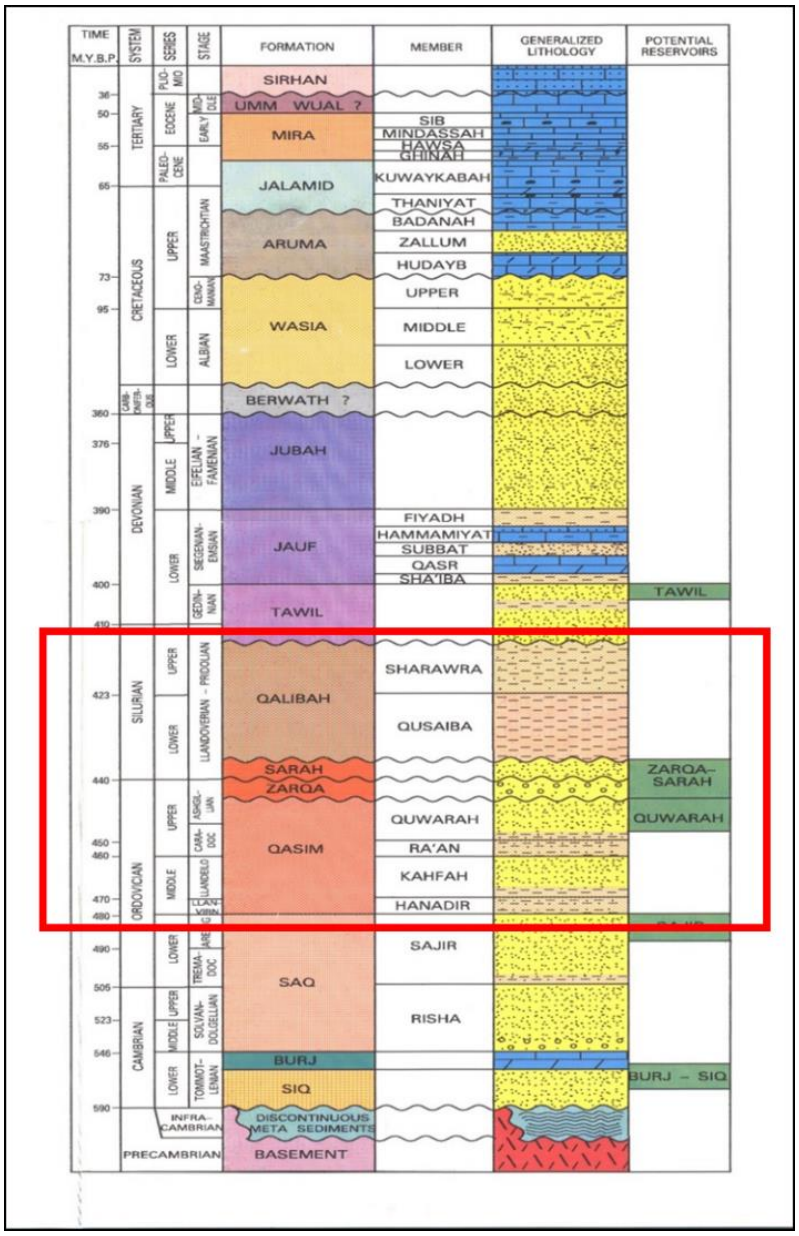

Figure 1.4. Generalized Stratigraphic Column in North West Saudi Arabia from the Saudi Stratigraphic Committee (2013)

we have learned from the Serri field stratigraphic geology that formations contain shale lithology. This lithology will affect the wavelength of the sent elastic wave producing anisotropy which will be discussed further in chapter 5. Paradigm Geodepth 15.0 software is the primary software used to carry out the study.

The full 3D seismic block was acquired in a 50 degrees angle and has 550 inlines and 887 xlines with 25 meter spacing over an area of 303 km^2. Table 1.1 and figure 1.5 show the survey parameters and acquisition layout. The maximum fold of the data used for

Table 1.1 3D seismic survey parameters

Criteria	**Value**	**Criteria**	**Value**
Area (km^2)	303.6	**Max. Fold**	4000
Year	2004	**Max. Offset (m)**	7000
Sweep Type	Vibroseis	**Samples**	1251
Shots	32,394	**Sample rate (ms)**	4
Receiver Stations	47,892	**Time Length (ms)**	4000
Receiver Spacing (m)	50	**Inlines (IL)**	550
Traces	125,000,000	**Xlines (XL)**	887
Max. Channels	4000	**IL/XL Spacing (m)**	25

seismic imaging is 4000 with irregular offset distributions. This will be one of the challenges due to the lack of number of traces in the near and far offsets (Figure1.6)

The shot gather shown in Figure 1.7 was acquired between inlines 1705 - 1800 and xlines 5258 – 5408. It could simply be inferred that the seismic data has a poor signal to noise ratio. The events are imbedded under the noise indicating that the reflective energy is extremely weak. This could be due to the acquisition parameters used in acquiring this survey. The surface geology in some areas is composed of basaltic layers. A different source such as dynamite would have been more efficient. However, this will add a challenge to the processing especially in picking the initial velocity vertical functions which will be discussed in more details in chapter 2.

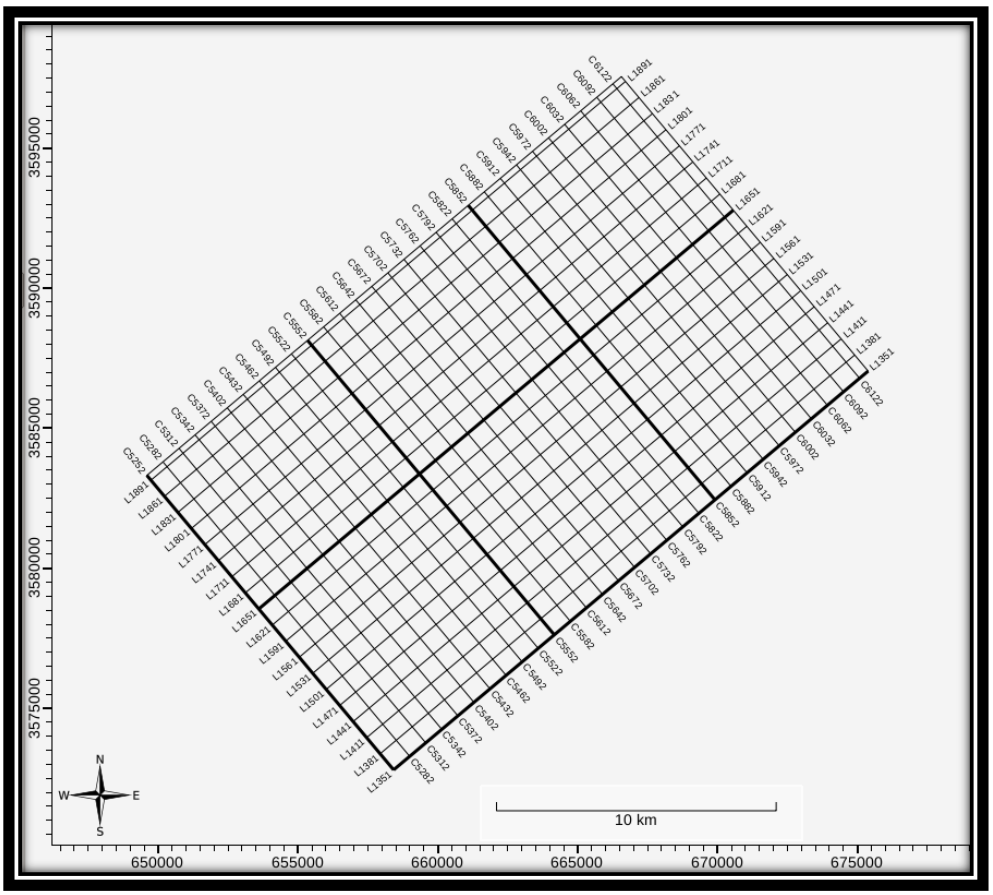

Figure 1.5 Survey layout: inlines vs xlines view of the 3D seismic block

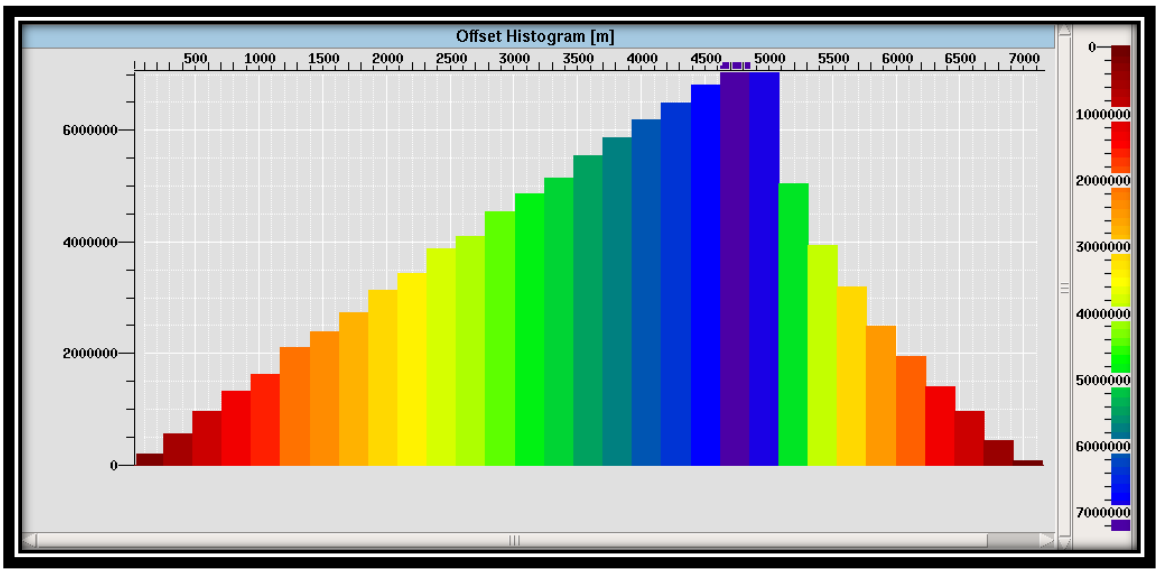

Figure 1.6 Offset histogram of the input dataset

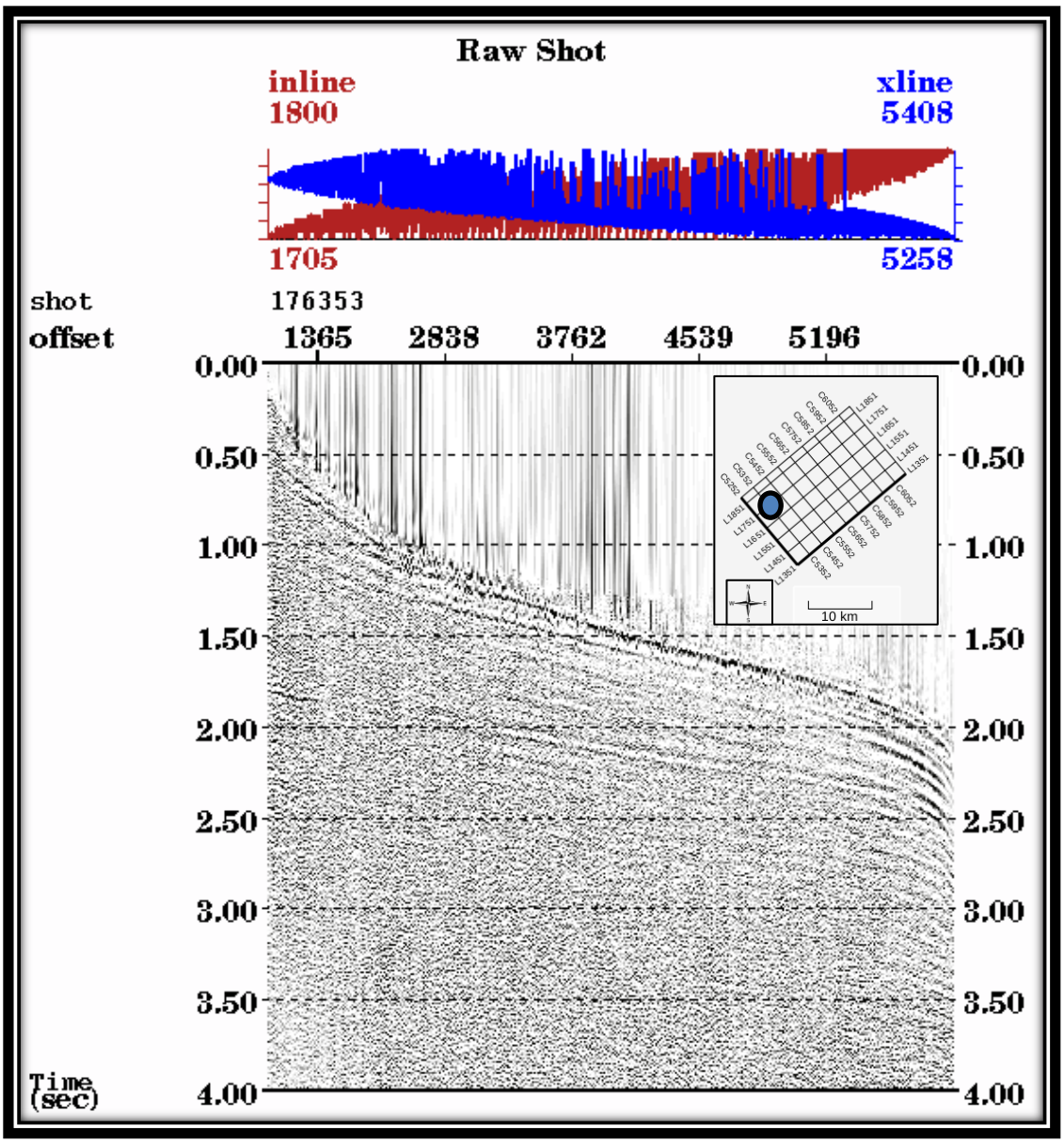

Figure 1.7 Input shot gather example

This shot gather was selected to analyse the spectral frequency of the seismic. The green area square inside the shot gather at the left bottom of figure 1.8 is where the spectral frequncy analysis was performed where the blue circle indicates where this shot was acquired in this survey. It can be deduced that the frequencies in this data range from 5 Hz to 80 Hz where it is around 30 - 60 Hz at highest amplitudes. However, this study will not carry out any signal processing and will merely focus on imaging.

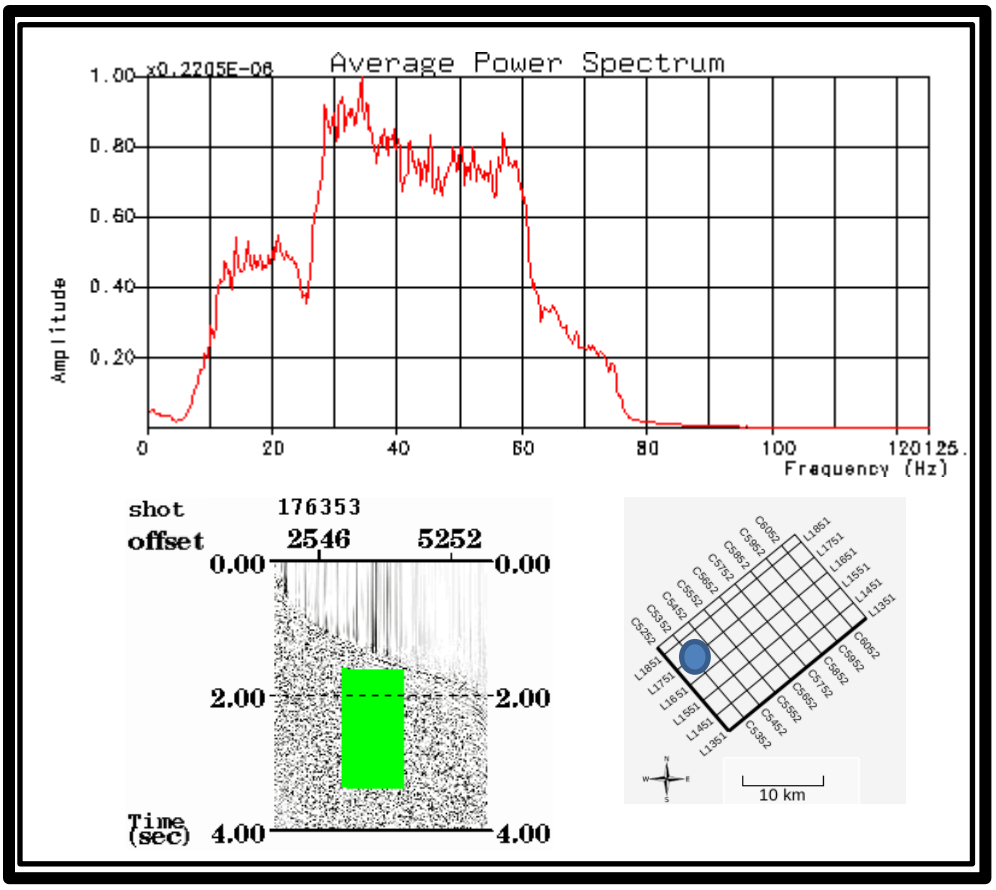

Figure 1.8 Shot Gather Spectral Frequency Analysis

The data have been processed in the Time Processing Department in Saudi Aramco and was preconditioned to depth processing. The following are the major time processing steps done on the data set before it was written to a *segy*:

- COG noise suppression.
- Statics: GeoTomo, Wave-equation Datuming.
- Residual 3D statics analysis (24ms).
- Trace editing.
- Common Offset Noise Suppression IL/XL: LFK/ FXDECN/ Sort.
- Residual 3D statics 48ms.

There are plenty of wells drilled in the area, and only 6 wells were accessible and provided for this research. All of these wells had targeted lower Silurian and upper Ordovician sandstone reservoirs stratigraphically related to the Sarah paleocurrent channel as well as Qasim formation. The wells contain gamma ray, density, neutron, S-wave sonic and P-wave sonic logs. The well logs will be useful tools to pick TWT horizons and identify formations on the seismic section and also calibrate the depth maps to wells during the velocity model building. Moreover, slowness attributes from the sonic are going to be significant inputs in determining the anisotropic parameters required to create an anisotropic velocity model.

The goals of this thesis was approached through a sequential practical work. Figure 1.9 shows a flow chart that displays the sequence of major steps that were used in order to achieve the objectives of this research.

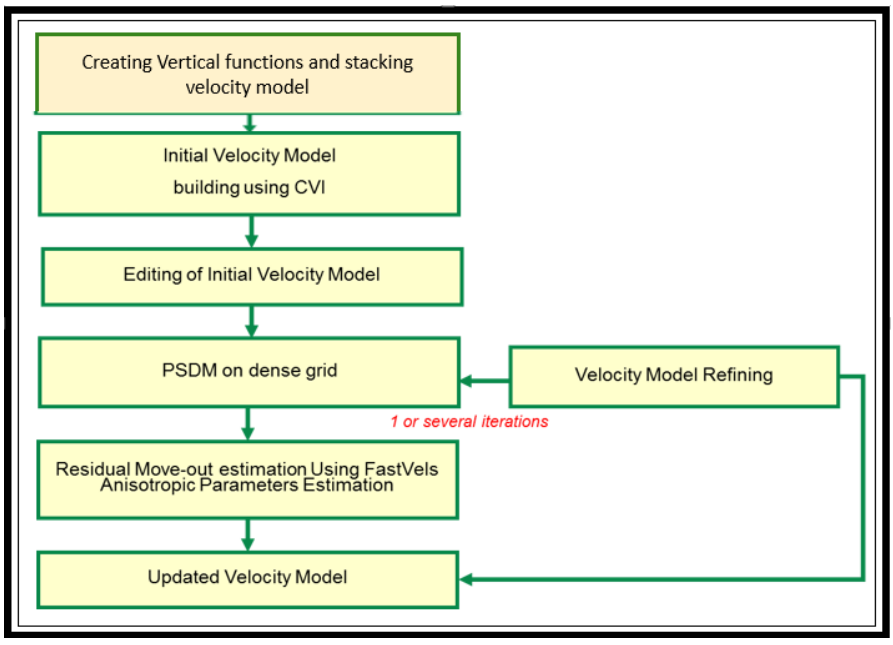

Figure 1.9 Workflow of Velocity Model Building and PreSDM

Chapter 2

Preliminary Seismic Velocity Analysis

2.1 Seismic Velocity Model Representation

A seismic velocity model is a set of geological layers separated by interfaces, horizons, fold, and transition zone. In sedimentary geology, velocity within each layer is characterized by a smooth laterally varying distribution, which normally increases monotonously with the increasing thickness of the layers. Generally, there are discontinuities in the velocity and density parameters which is known as reflection coefficients that occur across the interfaces. In sediments such as sand and shales velocities tend to change whereas it is normally homogenous in hard rocks such as igneous or carbonate rocks. (Upadhyay, 2004)

A velocity model can be represented as: (1) layer based model, (2) grid based model, and (3) hybrid model representation. In layer-based model, velocities are represented vertically by a piece-wise continuous function indicating the vertical changes of velocity within and across the layers. In grid-based model, velocities are represented in a fine grid computed from lateral and vertical location whose dimension indicates the grid seismic resolution. Hybrid model represent velocities in a grid in every geological layer where the grid can be regular or irregular. The study area is interpreted to have low dipping

formations so in this thesis, the layer based velocity model will be used throughout the analysis. (Dekel)

2.2 Seismic Velocity Vertical Functions

The shot/offset gathers were first sorted by CMP/offset gathers in order to be able to pick reflections and correct for the normal move-out (NMO) (Figure 2.1). Paradigm software undertakes a CMP as the point of intersection of every inline and xline. Although the signal to noise ratio is still weak after sorting, it is slightly more coherent, and thus, initial vertical functions were picked by using the semblance velocity method. (Figure 2.2& 2.3) show a CMP before and after a vertical function being picked. The QC time gate in the bottom right corner shows how the time stack section behave after presenting those energies in the vertical function.

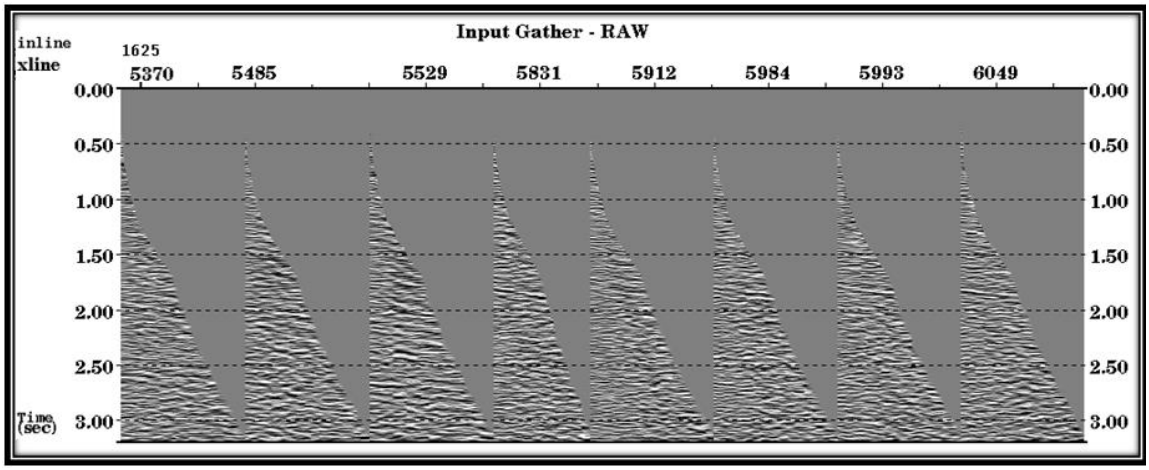

Figure 2.1: Multi gather view of raw data with automatic gain control AGC applied.

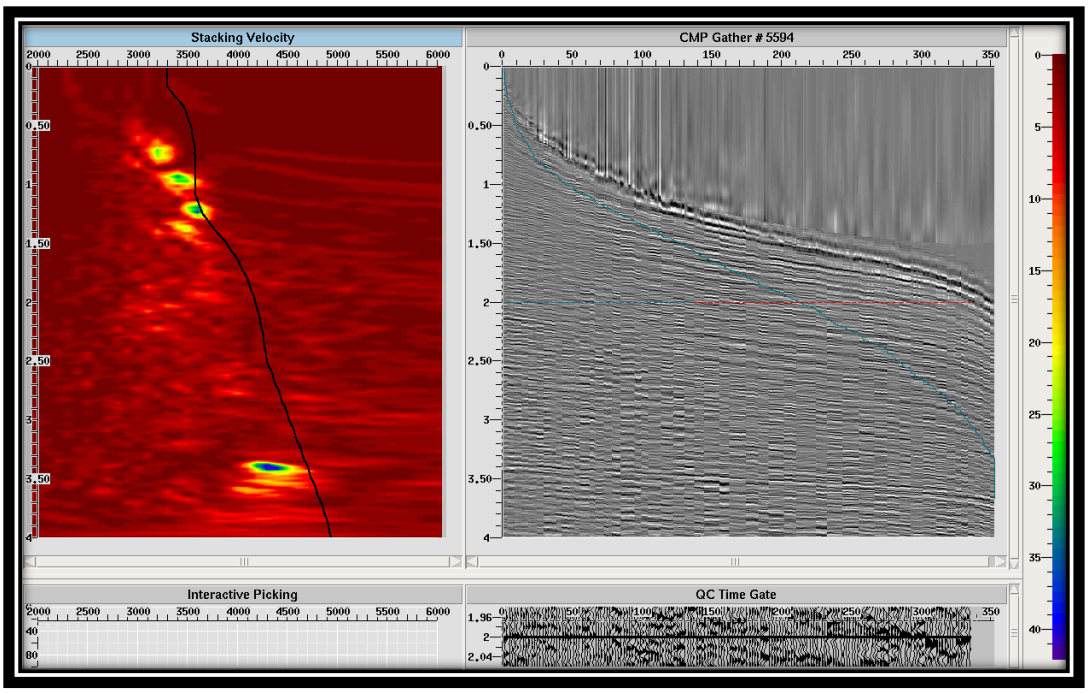

Figure 2.2 Example of a CMP input gather QC before picking a seismic vertical velocity function

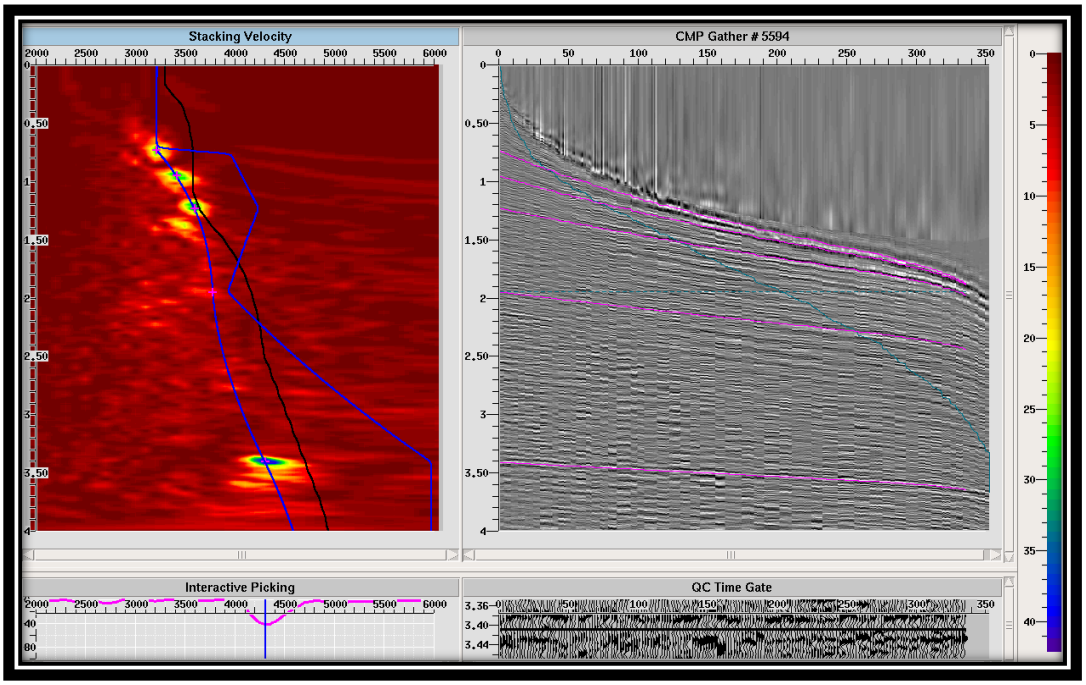

Figure 2.3. Example of CMP Input Gather QC after picking a seismic vertical velocity function where time gate shows more continuous reflections

In this application, vertical functions were picked every 20th CMP over the 3D volume. The graph in Figure 2.4 shows the initial vertical 1220 functions displayed in lines and points. A 2000 m smoothing operator was run while creating the stacking velocity volume. These vertical velocity functions will be used to create a stacking velocity section which will be used to perform a normal moveout correction to the gathers where time events will be brought back to t_0. The stacking velocities range from 2350 to 4900 m/s. It also can be deduced that the velocity does not always increase with time implying some velocity inversions throughout the seismic volume which will be more evident after generating interval velocities in the next chapter.

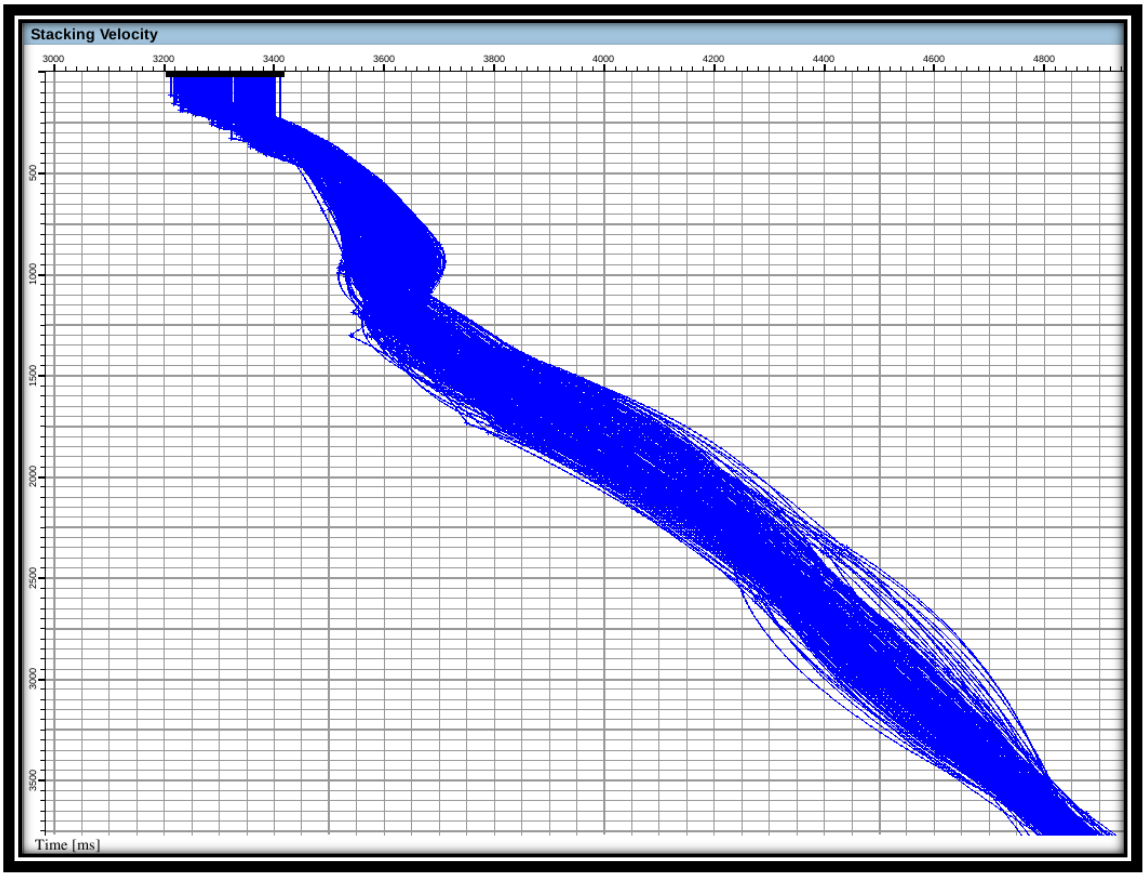

Figure 2.4. Display of vertical velocity functions points interpolated by lines.

The Serri field has a layered sub-horizontal stratigraphy with gently dipping horizons. However, a horizontal velocity analysis is needed in order to detect any lateral variations due to facies changes. After running a 3D automatic TWT picking of key horizons using the well markers, the TWT interpretations were loaded into the software and gridded separately. These time surfaces were used in hyperbolic stacking velocity analysis. Although the signal-to-noise ratio is unquestionably poor on all horizons, successful attempts were made to pick velocities. Figure 2.5 shows an example of a horizon velocity analysis before and after picking velocity. The QC time gate in Figure 2.5 shows little to no improvement in the image quality.

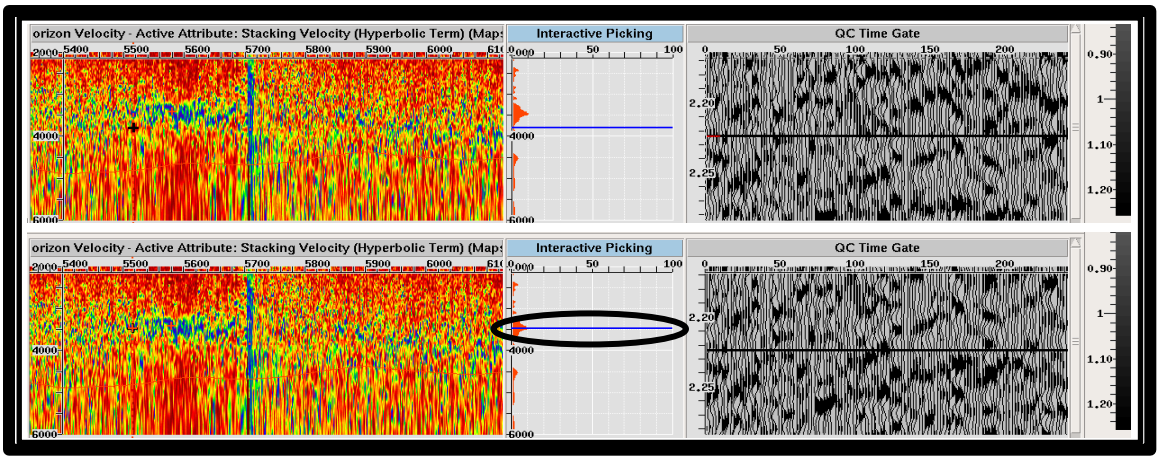

Figure 2.5. Horizon velocity analysis where top section is before picking the event whereas the bottom is after picking.

The horizon velocity interpretation were then left out and a moving average interpolation method was run to interpolate and grid the vertical functions, and create a layer based stacking velocity model. Figure 2.6 shows a 3D display of the stacking velocity volume while Figure 2.7 displays a cross section of the stacking velocity model along inline# 1627. TWT horizons were superimposed on the section to show the vertical and lateral behavior of the velocity. Preliminary observations from the velocity volume confirm

that the geology seems to have a layer-cake stratigraphy with little lateral complexities. However, there appear to be some vertical changes in velocity at ~1200 s TWT where it drops from 3500 m/s to 3100 m/s. In addition, although the velocity section has been smoothed, there are noticeable fluctuations of the velocity especially in the middle of the volume due to poor reflections.

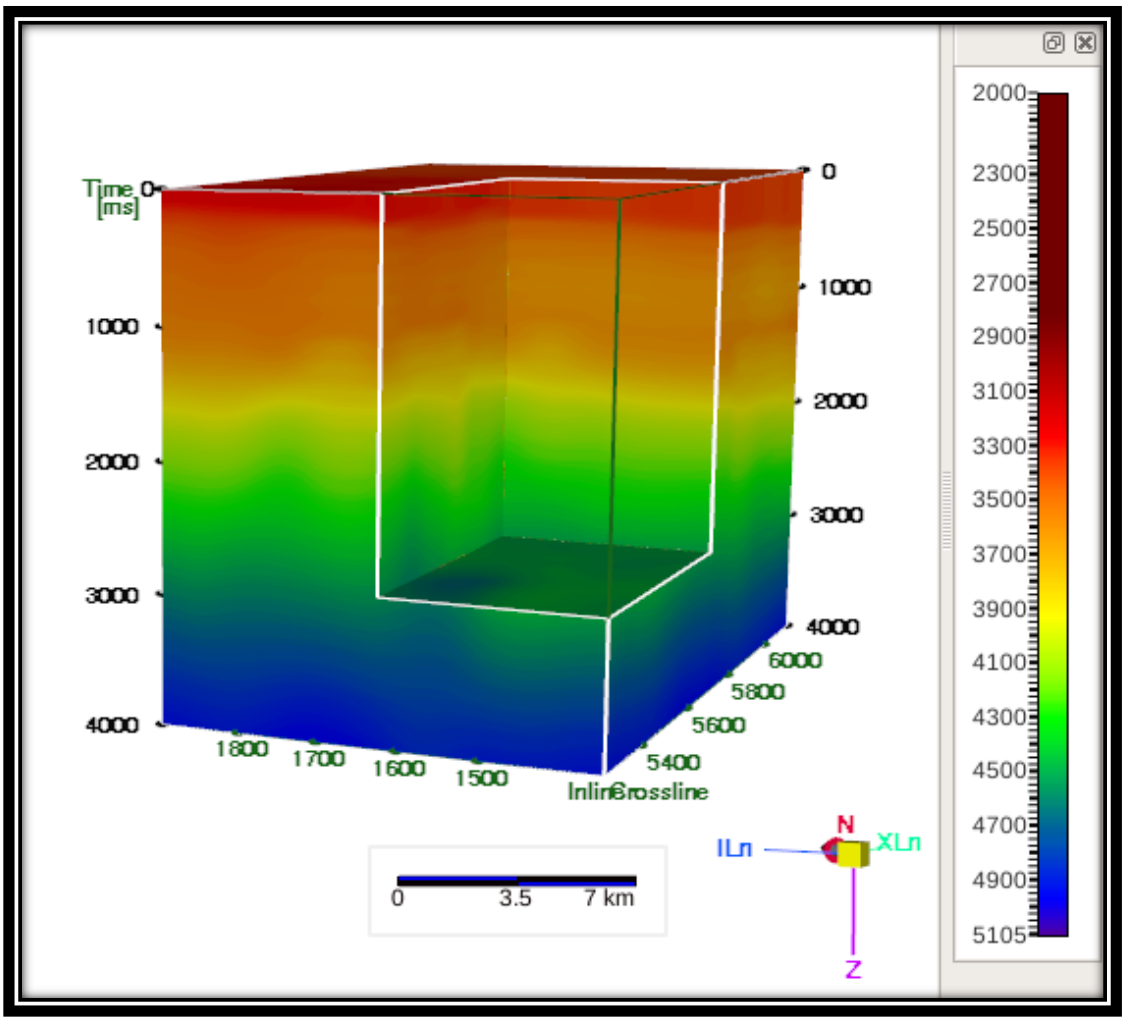

Figure 2.6. 3D Cube of the stacking average velocity volume

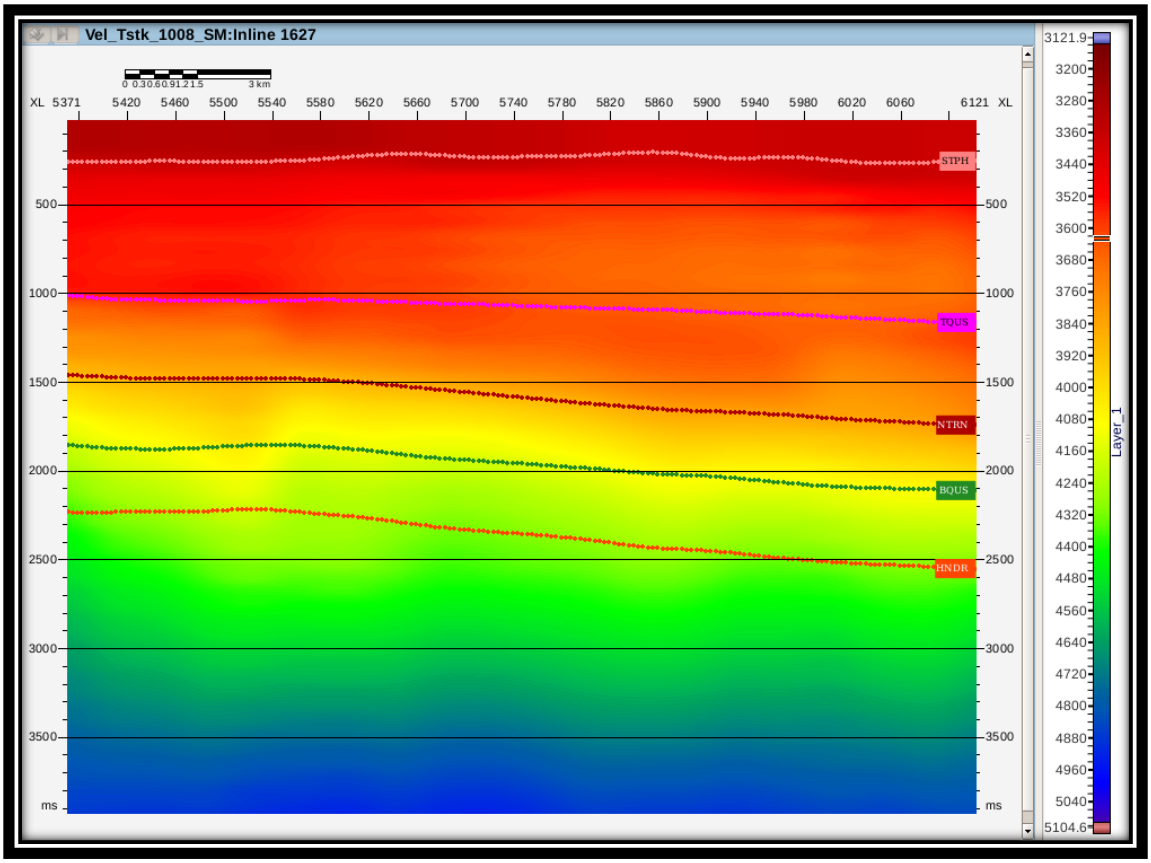

Figure 2.7: Stacking velocity section at IL1627

Using the stacking velocity volume above, NMO and stack modules were run to produce constant velocity stack (CVS) sections. Figure 2.8 shows the seismic section across inline# 1625. This stack raises a number of observations: (1) the seismic image has poor quality and the horizons seem to be discontinuous laterally, (2) the horizons show gentle slopes, (3) there is a hint of some structural features such as low degree anticlines and faults. All of these preliminary interpretations are indications of a need for further processing which will be discussed in more details throughout this thesis.

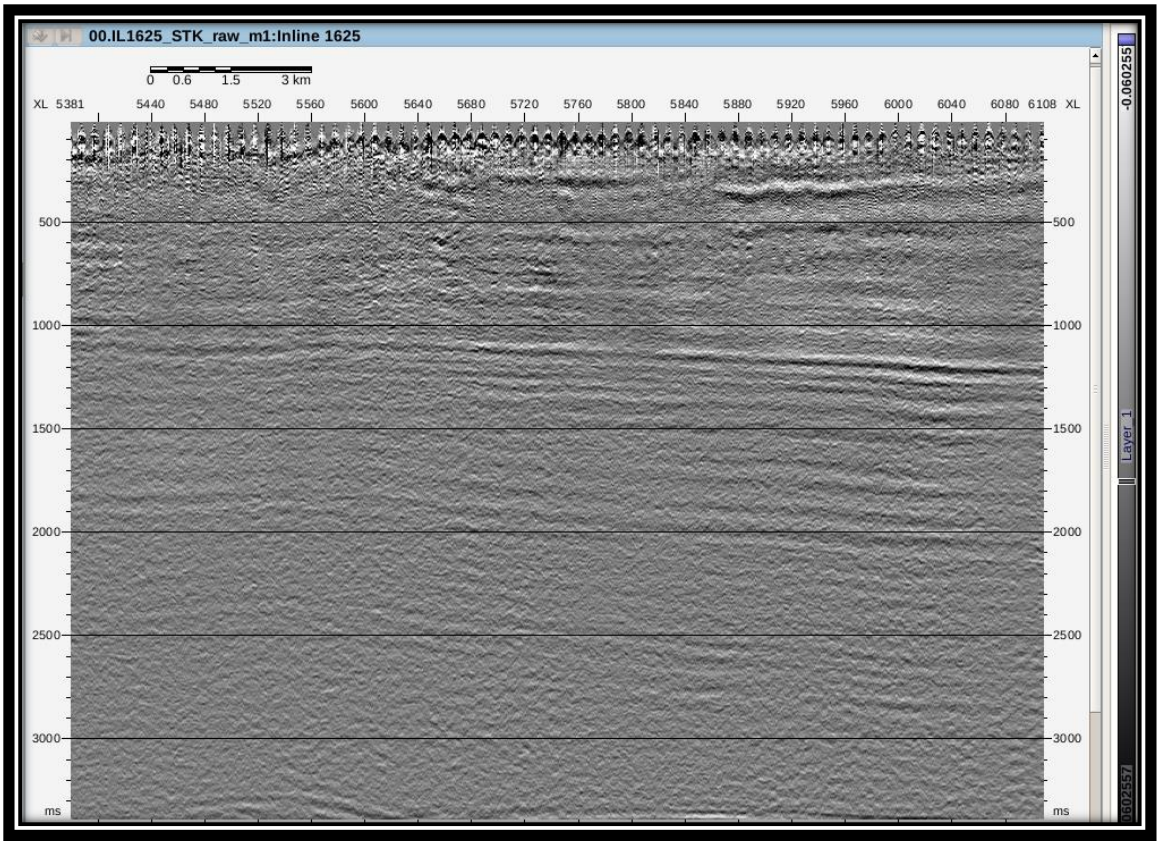

Figure 2.8 Seismic Stack Section of IL 1625

Chapter 3

Constrained Velocity Inversion Velocity Model Building

3.1 Constrained Velocity Inversion: Theory

CVI is a stable inversion method to create geologically constrained instantaneous velocities from a set of sparse, irregularly picked stacking or root mean square-velocity functions (RMS) in vertical time. A stacking velocity is defined as a parameter for the hyperbolic curve that best fits the moveout of reflection times over source-receiver offset. Inversion is done in four stages: establishing a global initial background-velocity trend, applying an explicit unconstrained inversion, performing a constrained least-squares inversion, and finally, fine gridding. (Harlan, 1999)

RMS Velocities are assumed to be equivalent to stacking velocities. Let a one dimensional vector $\underline{s}$ be a single function of squared stacking slownesses, and $\underline{v}$ for interval velocities. The RMS average of $\underline{v}$ is written in a discrete function as:

$$1/s_j = \frac{1}{j+1} \sum_{k=0}^{j} v^2{}_k \tag{3.1}$$

Dix equation is an explicit inverse of RMS and written as:

$$v_k = \sqrt{\left(\frac{k}{s_k} - \frac{k-1}{s_{k-1}}\right)} \tag{3.2}$$

However, velocity inversions in stacking velocities could lead equation to fail when required to take square root of negative numbers. A small perturbation Δv_k of interval velocity results in the following perturbation Δs_j of squared stacking slowness.

$$\Delta s_j = [-\frac{2\,s^2{}_j}{j+1}] \sum_{k=0}^{j} v_k\, \Delta v_k \tag{3.3}$$

So, for a constrained inversion a linearization of the Dix equation is written as:

$$\Delta v_k = v_k \sum_{j=k}^{\infty} [-\frac{2\,s^2{}_j}{j+1}]\, \Delta s_j \tag{3.4}$$

Damped least-squares is used to balance data errors with minimal complexity in the model. It works by defining a linear smoothing operator $\widetilde{B}$ and vector $\underline{w}$ to contain the smoothing coefficients:

$$v_k \equiv \sum_i b_{k-i}\, w_i \equiv (\widetilde{B}\ .\ w)_k \tag{3.5}$$

After convolving indirectly over all spatial indices (5) the best coefficients of $\underline{w}$ should minimize the following function:

$$\left\{ s_j - \left[\frac{1}{j+1} \sum_{k=0}^{j} (\tilde{B}\ .\ w)^2{}_k \right]^{-1} \right\}^2 + \in \sum_k w^2{}_k \tag{3.6}$$

An error Δs could result from producing a particular set of square stacking slownesses $\underline{s}$ from a partially optimum set of coefficients $\underline{w}$. The following equation is defined at the best perturbation of coefficients with linearization from (3).

$$\left[\Delta s_j - \frac{2\,s^2{}_j}{j+1} \sum_{k=0}^{j} (\widetilde{B}\ .\ w)_k (\widetilde{B}\ .\ \Delta w)_k \right]^2 + \in \sum_k (w_k + \Delta w_k)^2 \tag{3.7}$$

As a final optimization, early iterations begin with a large smoothing operator which is reduced after a full optimization over a simplified interval velocity (Harlan, 1999).

The method is primarily designed for building initial velocity models for curved-ray time migration and initial macro models for depth migration and tomography. It is mainly applicable in regions containing compacted sediments, in which the velocity gradually increases with depth and can be laterally varying. The method can be applied to create a new velocity field or to update an existing one (Koren and Ravve, 2006).

3.2 Constrained Velocity Inversion Model

3D models were created to contribute to the constrained velocity inversion. The stacking velocity volume from the previous chapter was used as input to create the first initial CVI model. More weights of 60% were applied to trend whereas 30% of weights will be used from data due to the noticeable trend and clear poor quality of the data. Figure 3.1 shows the input to CVI and the resulting interval velocity volume in depth.

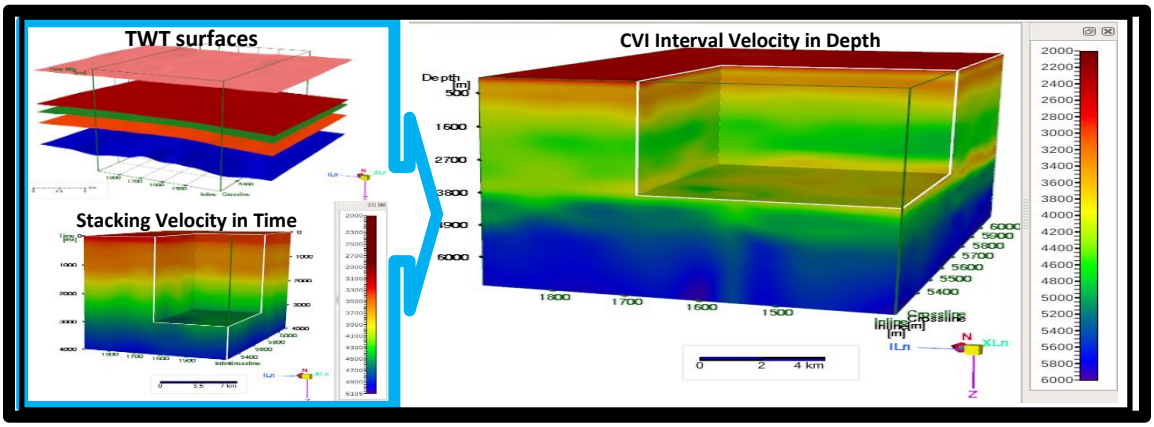

Figure 3.1 3D view of three inputs to create the constrained velocity model. Top left TWT surfaces, bottom left is the stacking velocity volume, right is the CVI model.

A cross section of the CVI velocity volume in depth along inline # 1627 is displayed in Figure 3.2. Interval velocity depth maps were extracted from the volume and used to convert to depth the TWT horizons. Then, they were superimposed in the section below to QC the resultant velocity model. at 4,000 m. the velocity drops down. Velocities increase significantly at the lower Base Qusaiba formation. Hanadir formation at a depth 4500 – 5,200 m shows a fluctuation in lateral velocity values between 4,800 m/s to 5,800 m/s as we go SW. This layer based velocity volume overall contains a detailed representation of the subsurface geology. Therefore, it will be used to create a travel time table to perform the first run of prestack depth migration (PreSDM).

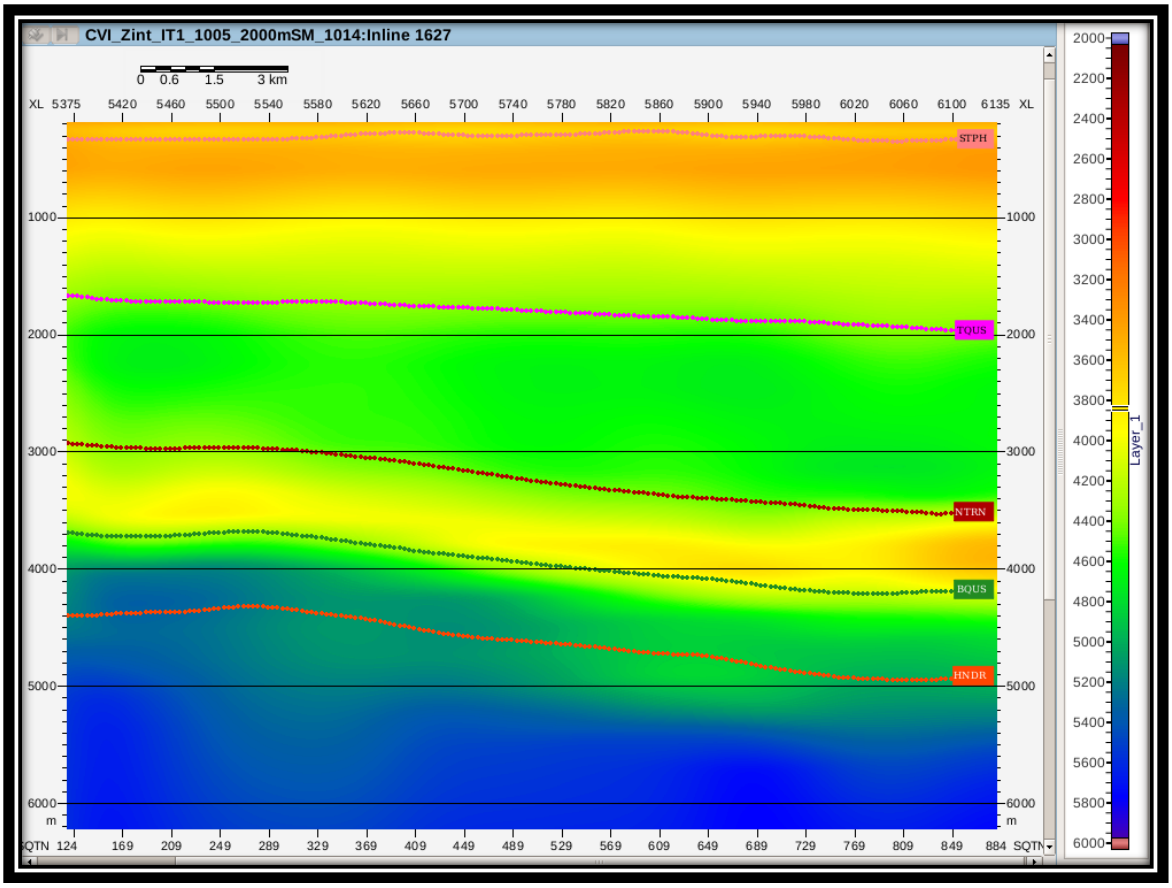

Figure 3.2 CVI velocity section view at IL1627

The velocity section displayed in the Figure 3.2 above provides a more detailed information about the variation of the velocity in the medium and we can draw several conclusions especially looking at the very noticeable inversion of velocity at 3740 m where the velocity drops from 4800 m/s to 4000 m/s. This event could relate to an igneous body intrusion at this depth. The horizons on the section represent the depth maps converted from time using the stacking velocity model. In addition, the section outlays a lateral change in velocity along the Hanadir formation at the bottom of the section which is known to be composed of shales (Saudi Stratigraphic Committee, 2013)

Chapter 4

Kirchhoff's PreSDM Migration

4.1 Kirchhoff's PreSDM Migration - Theory

Prestack depth migration is a useful tool for positioning the geological events at their true position in the subsurface media. There are many depth migration algorithms used widely in the oil and gas industry, and all differ based on computation requirements and mathematical operations. Depth migration has also become an important technique in velocity model building. In this research, our objective was to develop an anisotropic velocity model that is a product of lateral and vertical variations of velocities of the propagating waves in the subsurface.

Kirchhoff's ray-tracing algorithm was used to carry out the prestack depth migration.in developing this model. In Kirchhoff PreSDM traveltimes are computed by ray tracing performed through complex 3D models. Data are primarily stored into several common-offset 3D volume. Each of these volumes is 'regularized' to contain traces of comparable fold and possible azimuth range, placed on a regular grid in x and y Every imaged point are considered as diffraction point D; traveltimes and weights are computed for each imaged point by explicitly shooting dynamic rays through this 3D velocity model in depth (Figure 4.1). Thus, reflectivity in any point D is computed by a weighted sum along its corresponding diffraction surface; the limits of the diffraction surface are governed by the aperture of the migration operator. In other words, the diffraction surface

for a given point D at depth z, aperture x and offset 2h is computed from the sum of the traveltimes t_s along the ray from the shot to the image point plus the traveltime t_r from the imaged point to the receiver (Robein, 2010).

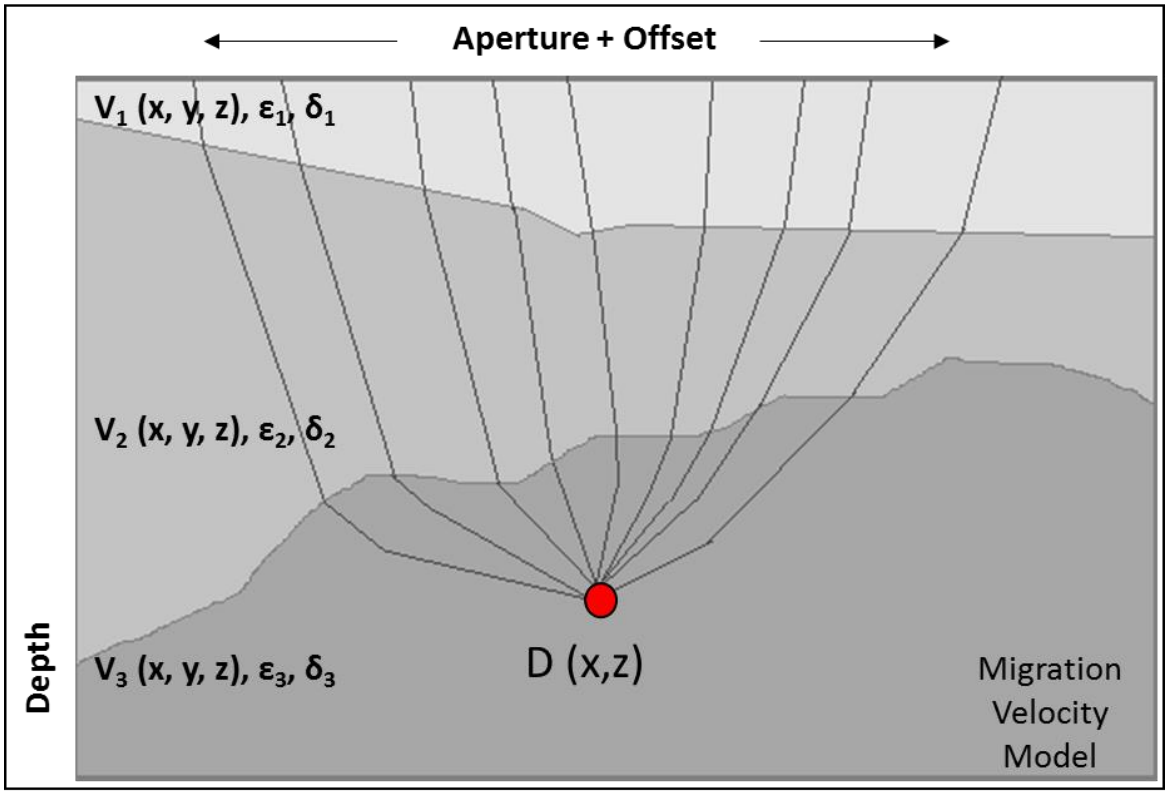

Figure 4.1. Seismic raypaths from a diffraction point D in a schematic anisotropic migration velocity model in depth (from Robein, 2010).

4.2 Isotropic Kirchhoff PreSDM Using the CVI model

The interval velocity model in depth created in the previous chapter contains isotropic information about the geological layers of the study area. It was used to build the travel time tables based on the wavefront Kirchhoff's computation technique. Subsequently, a depth migration was run on the gathers using an aperture of 2000 m. Offsets were limited to 5000 m during the migration because (1) the traces beyond offsets above 5000 were limited, (2) migrating data with shorter offsets requires less computation

power. Figure 4.2 shows several migrated gathers along IL1625. These gathers are converted back to time using the CVI velocity model.

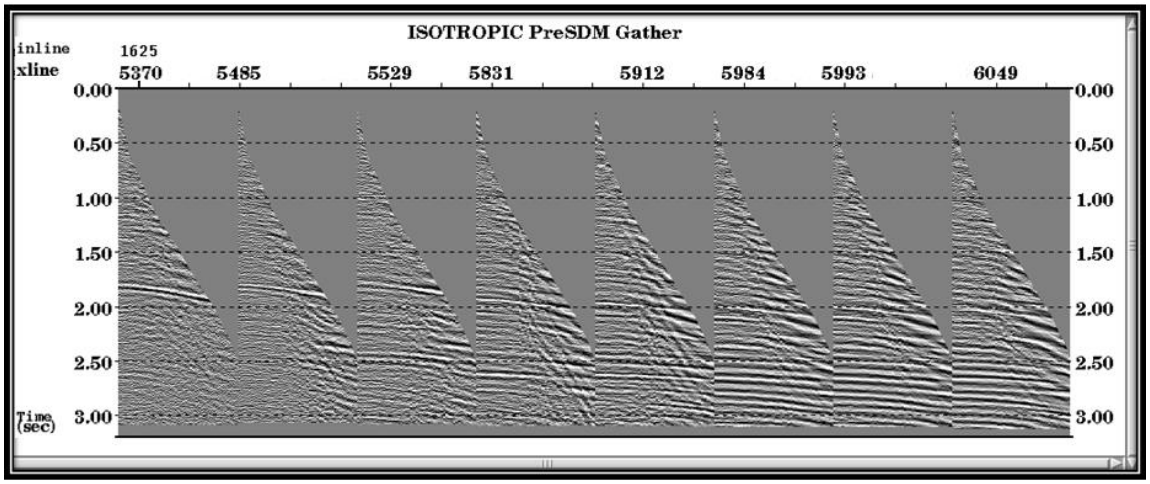

Figure 4.2 Multi gather view of isotropic PreSDM depth to time gathers with 300 AGC.

The depth migrated gathers (scaled to time) in Figure 4.2 correspond to the input gathers shown in Figure 2.1 in Chapter 2 with the difference that here is after PreSDM which will be discussed further in Chapter 6. The PreSDM results show how clear the reflections that were imbedded within noise became after the depth migration as a consequence of boosted signal to noise ratio.

Figures 4.3(in depth) and 4.4 (in TWT) are cross sections of the stacked volume along IL1625 where Figure 4.3 is in the depth domain and Figure 4.4 is in the time domain after scaling the depth stack using the CVI velocity model.. Although the reflections in these new processed data appear to be more clear and continuous, they do not appear to be flat as expected throughout the migrated gathers. This is an indication that the velocity model did not correct the events at the far offsets likely being a sign of anisotropic effects. This will be examined in the next chapter.

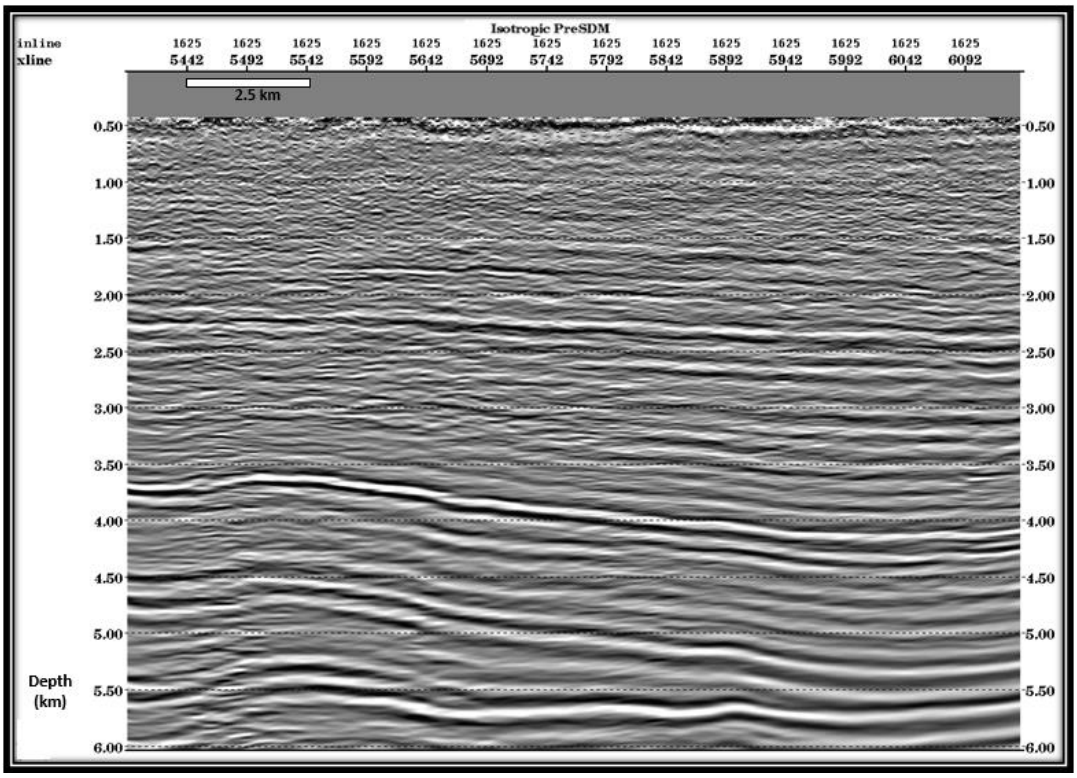

Figure 4.3 Seismic depth section at IL1625 after isotropic PreSDM.

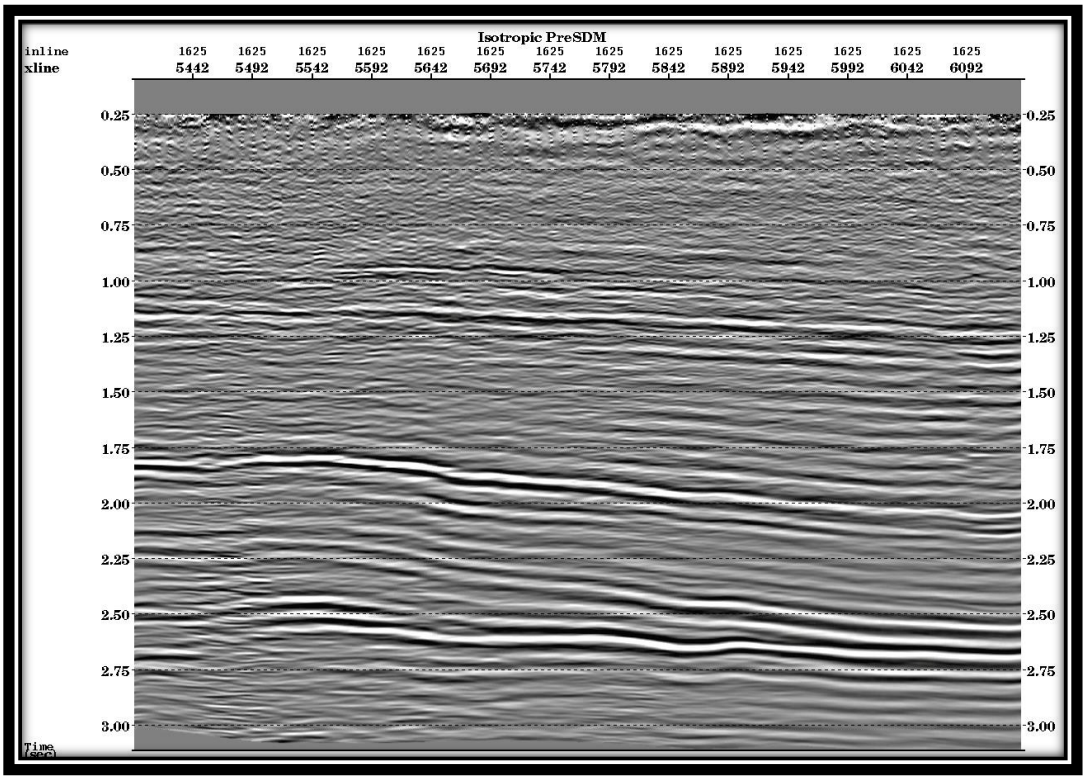

Figure 4.4 Seismic depth section at IL1625 after isotropic PreSDM converted to time

Chapter 5

Anisotropic Seismic Velocity Model Building

5.1 Concept of Seismic Anisotropy: Theory

In geophysical exploration, seismic waves used to image the subsurface travel through the earth and are reflected and refracted at sediment interfaces because the sediments have different velocity and density effects on the waves. The returning signals are what are recorded at the surface by measuring elapsed time from when the seismic signal is generated. The Earth is heterogeneous in nature, and thus, the propagation waves travel through different rocks in multiple direction at different speeds. This means that "seismic waves travelling in one direction relative to a vertical axis are going faster (or slower) than in other directions, an effect which varies aerially and with depth." (McBarnet, 2008).

Anisotropy is seen in almost all rocks affecting both compressional and shear waves in different ways. The directional and spatial effects of anisotropy can be difficult to distinguish when using only seismic data. Anisotropy arises from ordered heterogeneity at scales less than a seismic wavelength. There are different types of anisotropy and are classified based on the degree and effect of anisotropy (Tsvankin, 2001). This paper focused on the vertical transverse isotropy due to the horizontal layering structure of the study area. The elastic behavior of a layered structure would be like a homogenous transversely isotropic (T.I) medium having a symmetry axis perpendicular to the plane of

stratification (Upadhyay, 2004). The elastic modulus matrix for an anisotropic case in a vertical transverse isotropic medium (VTI) is derived firstly from Hook's Law which states that for elastic behavior strain is directly proportional to the stress producing it. So, we can express the following relationship

$$\sigma_{ij} = C_{ijk} e_{kl} \tag{5.1}$$

$i, j, k, l = 1, 2, 3$, where σ is the stress, C is the elastic moduli or stiffness constant, and e is the strain. The elastic modulus matrix for an anisotropic case in VTI medium is

$$C = \begin{bmatrix} C_{11} & C_{11} - 2C_{66} & C_{13} & 0 & 0 & 0 \\ C_{11} - 2C_{66} & C_{11} & C_{13} & 0 & 0 & 0 \\ C_{13} & C_{13} & C_{33} & 0 & 0 & 0 \\ 0 & 0 & 0 & C_{44} & 0 & 0 \\ 0 & 0 & 0 & 0 & C_{44} & 0 \\ 0 & 0 & 0 & 0 & 0 & C_{66} \end{bmatrix} \tag{5.2}$$

Values of the constants C_{11}, C_{13}, .. etc. may be calculated knowing the thicknesses and elastic constants of isotropic constituents of the medium. (Thomsen, 2002).

In an isotropic medium, where the velocity is constant, the wavefront of a point source can be seen as the envelope of the propagation of an infinity of plane waves (Figure 5.1). However, in an anisotropic medium where waves propagate at a phase velocity, the wavefront is still the envelope of plane waves, but propagate at phase velocity that depends on direction (Figure 5.2). In this example, we explain the parameters that characterize anisotropy in a given location (x, y, z) for P-wave propagation in a homogeneous subsurface. There are four parameters: phase velocity, the axis of symmetry that is vertical for vertically transverse isotropy VTI, and two Thomson's parameters ε and δ. The VTI model for phase velocity (Thomson 1986) is:

$$V_{p\,(\theta)} \approx V_{ver} \cdot (1 + \delta \cdot sin^2\theta \cdot cos^2 + \varepsilon \cdot sin^4\theta) \tag{5.3 a}$$

$$V_{hor} = V_{ver} \cdot (1 + \varepsilon) \tag{5.3 b}$$

$$V_{p\,(45^{\circ})} = V_{ver} \cdot (1 + 0.25 \cdot \delta + 0.25 \cdot \varepsilon) \qquad (5.3\ c)$$

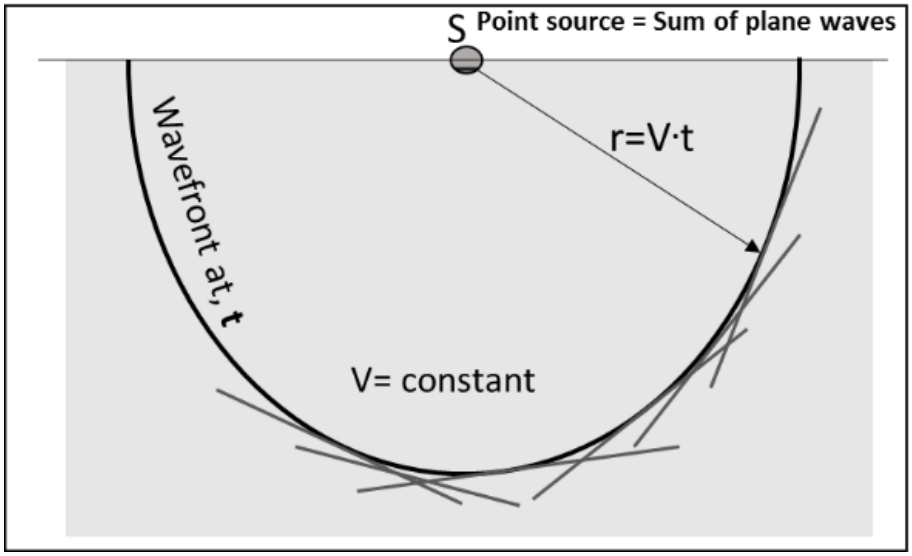

Figure 5.1 The wavefront envelope of planes in an isotropic case modified from Robein (2010).

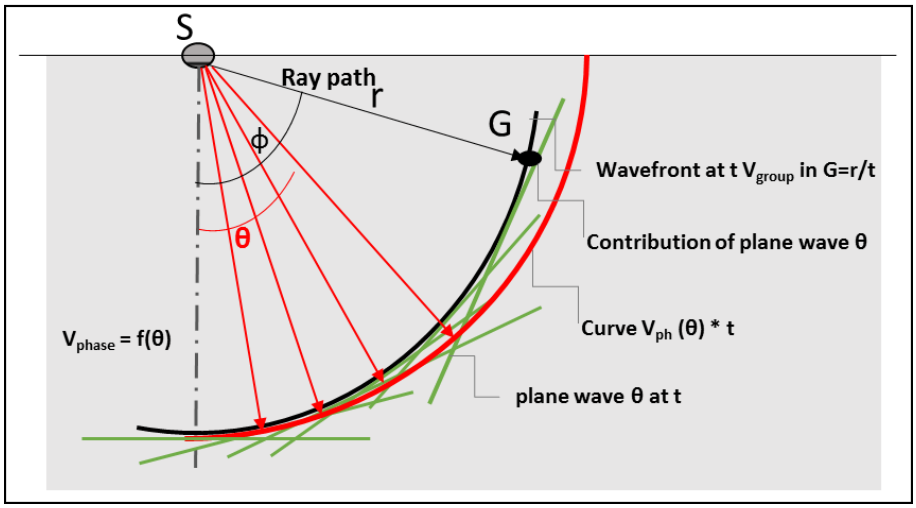

Figure 5.2 The wavefront envelope of planes in an anisotropic case modified from Robein (2010).

Snell's Law, which is a formula used to describe the angle of incidence and angle of reflection, can be illustrated using phase velocity to incorporate the anisotropy effect. (Figure 5.3). Here, the phase velocity which corresponds to the group velocity of the

incident ray is first computed from group and phase angles, group and phase velocity and anisotropic parameters ε and δ above the interface using the following equation:

$$V_{phase1} = V_{ver\,1} \cdot f(\theta_1, \varepsilon_1, \delta_1) \quad (5.4)$$

We can then apply Snell's Law to the phase velocity to compute θ_2 :

$$\frac{\sin\theta_2}{V_{phase2}(\theta_2)} = \frac{\sin\theta_1}{V_{phase1}(\theta_1)} \quad (5.5)$$

Then we can compute the group angle which gives the propagation direction (5.6 a) and subsequently the corresponding group velocity propagation (5.6 b; Robein, 2010):

$$\theta_2 = \phi_2\,(\phi = f(\theta, V_{ver}, \varepsilon, \delta) \quad (5.6\text{ a})$$

$$V_{Group2} = g\left(\theta, V_{phase\,2}, \frac{dV_{phase\,2}}{d_\theta}\right) \quad (5.6\text{ b})$$

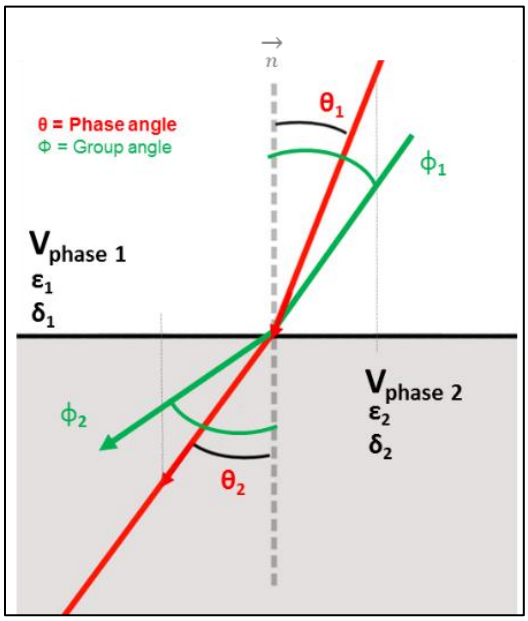

Figure 5.3. Snell's Law in anisotropic media modified from Robein (2010)

5.2 Anisotropic Velocity Model Parameters Estimation

Prestack depth and time migration need input from a velocity model, and therefore, they can handle the anisotropy effect but only if the anisotropic parameters are known. A

velocity layer based model can be defined as set of interfaces represented as depth maps digitized on a regular (x, y) grid, plus velocity functions within the layers between the interfaces parameterized as $V_0 + k \cdot Z$. The starting velocities V_0 and k (gradient functions) can be calculated from P- sonic logs and horizon markers for each formation. Vertical transverse isotropy (VTI) anisotropy is added to each layer through constant values of Thomson's parameters ε and δ. With the generalization of high-resolution tomography, we can now predict a field of ε and δ pairs modeled in a regular grid in conjunction with a predefined field of axis of symmetry. However, anisotropy parameters are poorly constrained by seismic data only. Estimating the epsilon and delta values has been a major challenge especially without some means of calibrating the anisotropy to some well information. Their inversion consequently requires imposing external constrains especially well data. Parameter delta (δ) defines the difference between a seismic near offset velocity V_{NMO} and a vertical velocity V_p and is defined as:

$$\delta = [V_{NMO}(0) - V_p(0)]/\, V_p(0) \tag{5.7}$$

Delta (δ) can be estimated from the difference between a well velocity and a seismic near offset velocity. This can be done by cross plotting well and seismic velocities as δ represents the bias. In this process, the parameter eta (η) can also be estimated. The Alkhalifah eta parameter (η) is an instantaneous anisotropic value that represents the non-hyperbolic moveout of the traces far offset (Alkhalifah and Tsvankin, 1995). While V_{NMO} corrects for a hyperbolic moveout, (η) can be estimated from the seismic interval velocities. Parameter epsilon (ε) affects long offsets and defines the difference between a horizontal and a vertical velocity and is defined as:

$$\varepsilon = [V_p(90) - V_p(0)]/\, V_p(0) \tag{5.8}$$

Epsilon (ε) can be estimated from parameter eta (η) for a given delta (δ) from (5.9; Alkhalifah and Tsvankin, 1995)):

$$\eta = \frac{(\varepsilon-\delta)}{1+2\delta} \qquad (5.9)$$

5.3 Building the Anisotropic Seismic Velocity Model

In this section, the interval velocity model created from CVI was updated and adapted to an anisotropic model through a number of processing steps. In the previous chapter, we noticed that the reflections were not subhorizontal especially at the far offsets. First, the depth migrated gathers were used to analyse and pick the residual moveouts to update the CVI velocity model. Figures 5.4 and 5.5 show an example of the horizon moveout effect on the QC depth gate. The horizons of residuals were then used to update the velocity volume.

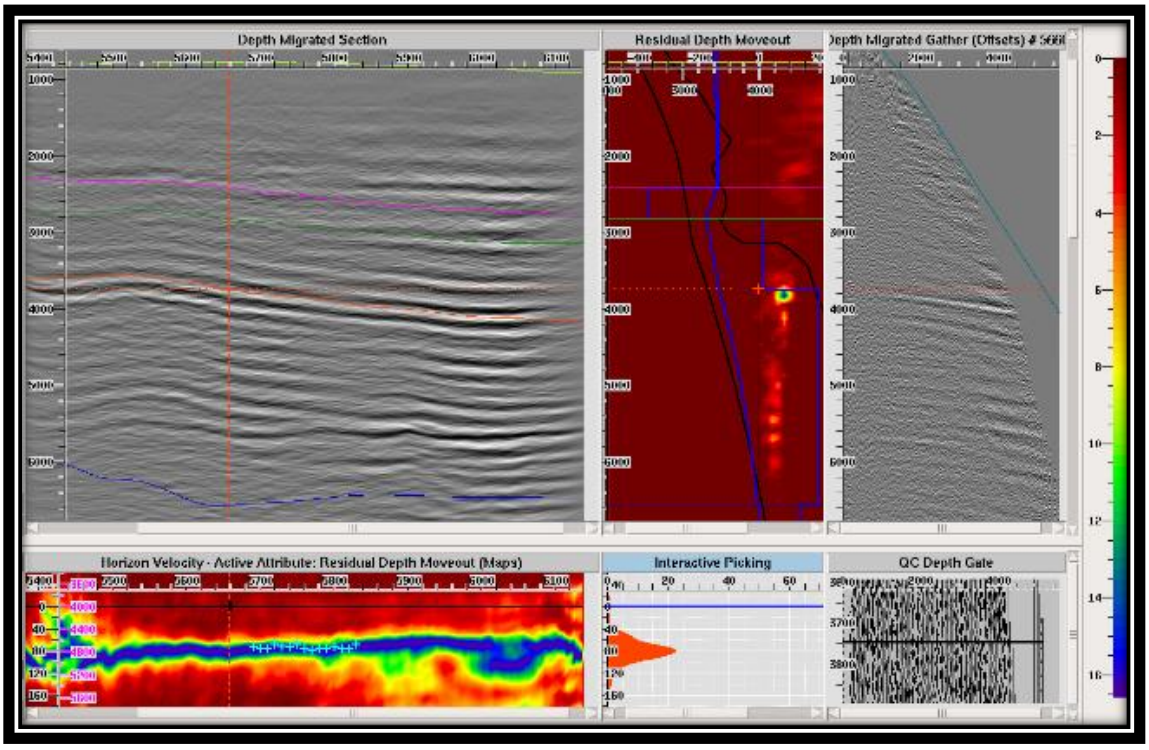

Figure 5.4 Horizon residual moveout analysis (before)

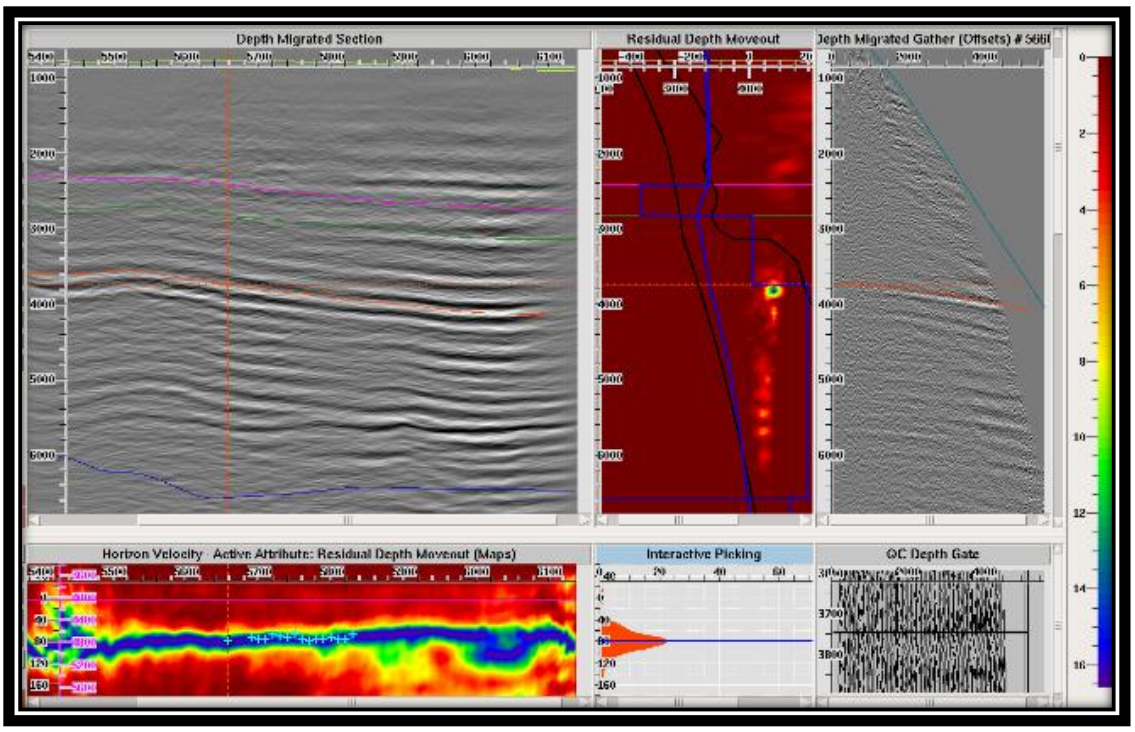

Figure 5.5. Horizon residual moveout analysis (after)

FastVel is a tool to pick the NMO residual moveout at far offsets where NMO cannot move the reflector back to t_0 using the isotropic velocity. These moveouts were run in a batch mode targeting all horizons, and fastvel moveout volume was created as shown in figure 5.6. This residual moveout volume is in depth and indicates locations where the seismic gathers cannot be corrected at far offsets using the current velocity model. In this example, the moveouts are large between depths 2000 m to 4000 m. These geological layers are correlated to shale deposits within sediments which are a primary source of anisotropy. Also, the lateral variations in the moveouts indicate a lateral change in facies. I extracted, therefore, the velocity of the base Qusabia formation to track the lateral changes in velocity. Figure 5.7a is a horizon slice of the base Qusaiba formation interval velocity. These particular locations were used to in calculating the anisotropic parameters ε and δ from the sonic well logs from well# 1. From the previous section, we learned that delta δ can be

estimated by cross plotting the NMO seismic velocity and the p-velocity from the sonic well log. Figure 5.7b shows extracted velocity vertical functions, picked every 50 CMP, from the interval velocity with depth (CVI model), and also the well p-velocity. At Qusaiba formation, the p-velocitywell.is 3578 m/s while the seismic velocity is averaged to be 3169 m/s. From δ equation (5.7), δ is calculated to be 0.11 which indicates the magnitude of the near offset effect of anisotropy. Alkhalifah η parameter is estimated from the seismic interval interface at Qusaiba formation where moveouts are clearly visible, and η is determined to be 0.25. Replacing η and δ in equation (5.9) results in an epsilon (ε) value of 0.20. Epsilon is, according to Thomson, "the fractional difference between vertical and horizontal P velocities; i.e., it is the parameter usually referred to as 'the' anisotropy of a rock" (Thomson, 1986). These parameters values are usually positive because velocity is usually faster along bedding.

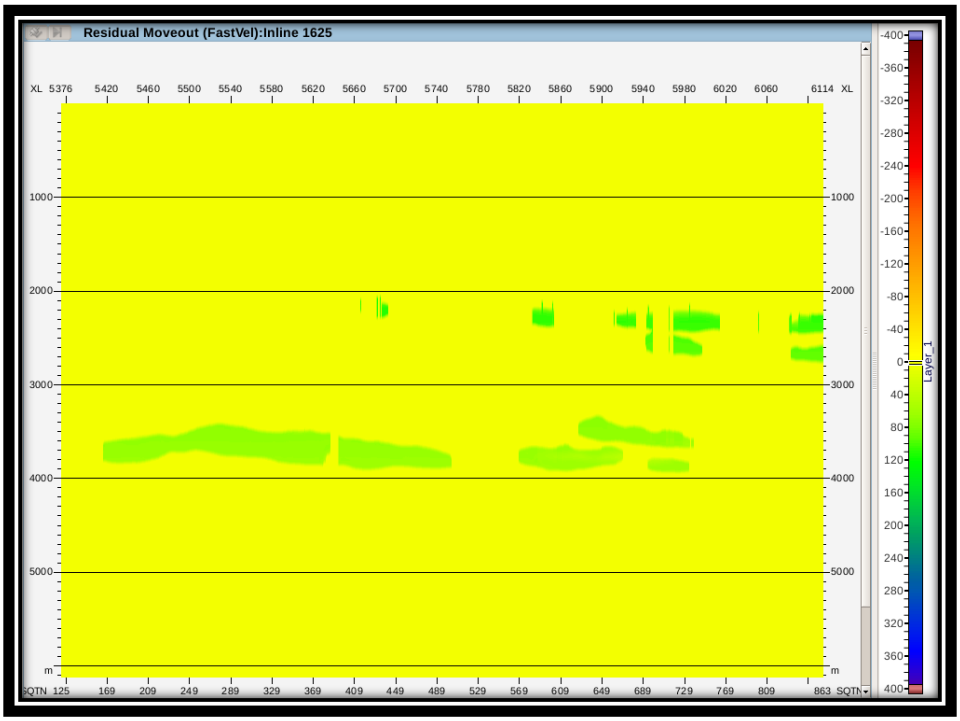

Figure 5.6 FastVel residual moveout section at IL 1625.

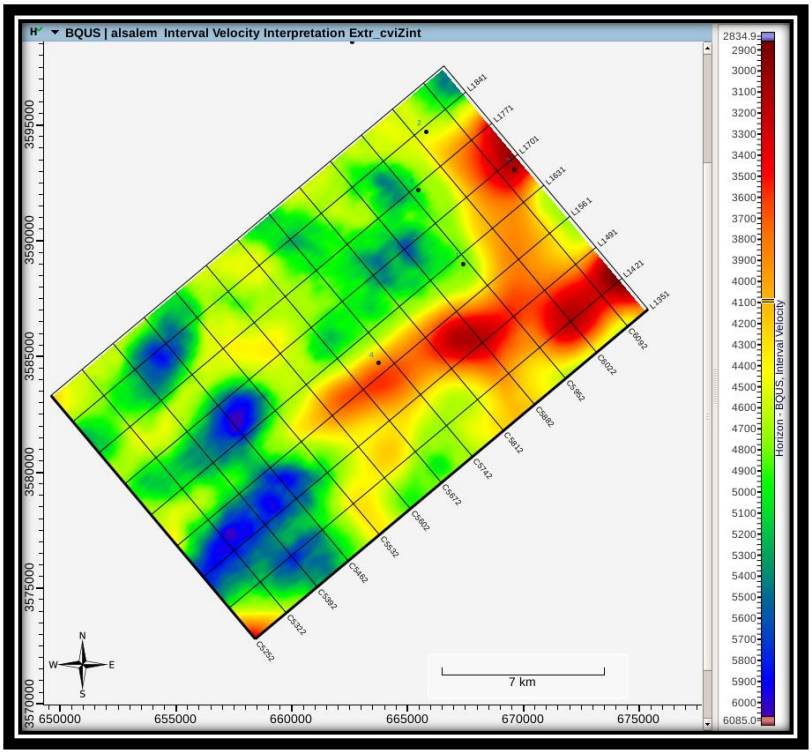

Figure 5.7a Base Qusaiba Formation interval velocity horizon slice

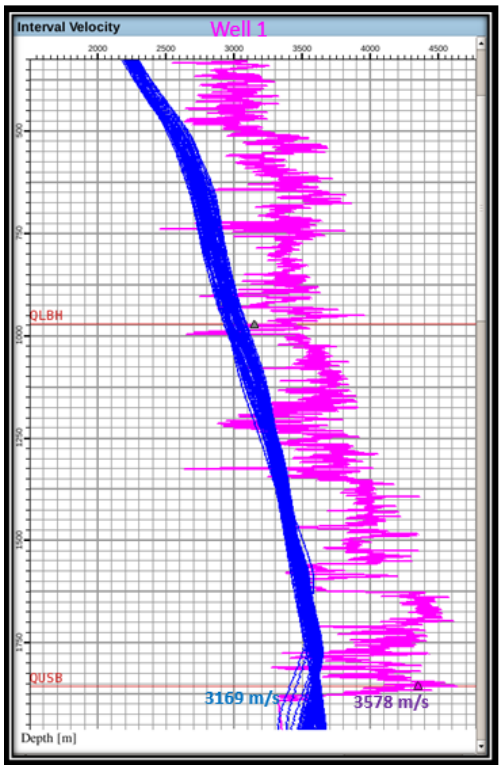

Figure 5.7b Seismic velocity & Well 1
P-wave velocity cross-correlation.

After estimating the anisotropic parameters from the wells, another investigation of these parameters was done by using the migrated seismic data. Here, I ran a horizon residual analysis of delta (δ) and epsilon (ε). intervals on top the Qusaiba formation and Hanadir formations which are the interfaces with high residual moveouts events (Figure 5.8 & 5.9). The moveouts from Figure 5.6 were overlaid on the depth migrated section showing in left top corner in Figures 5.8 & 5.9 in order to hint the locations where anisotropy is affecting the near and far offset of the data. The semblance of interval delta, as appears in the left bottom corner in Figure 5.8, shows that (δ)values range from – 0.2 – 0.4, however, the average value is around 0.14 which is relatively close to the 0.11 calculated parameter value from the sonic log.

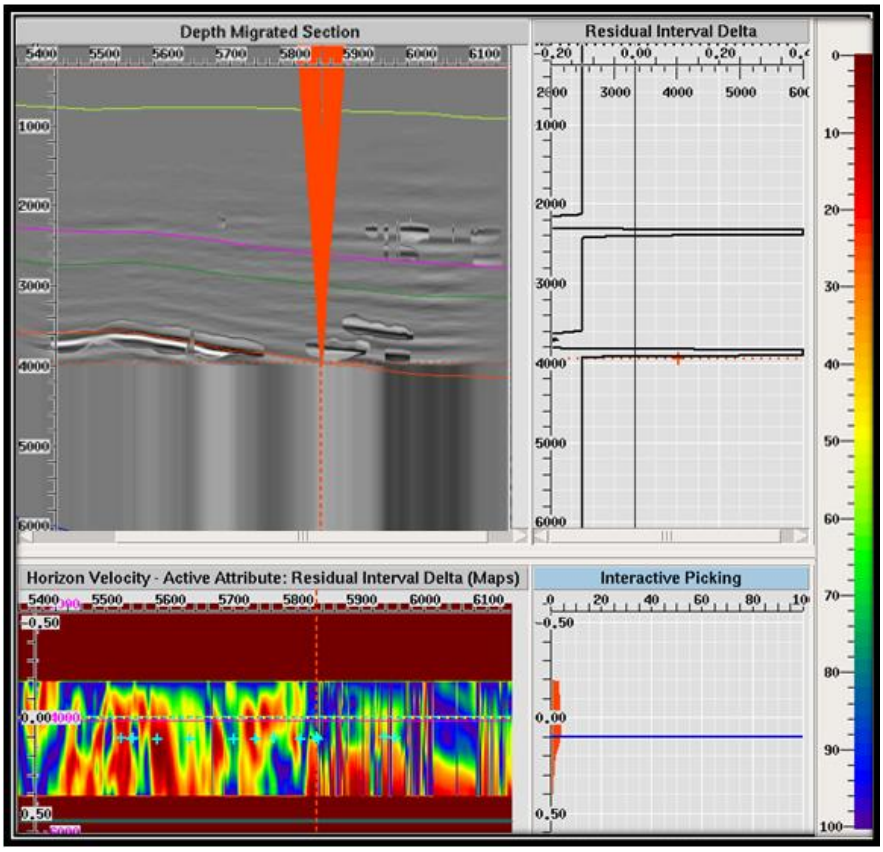

Figure 5.8. Residual analysis showing on bottom left corner interval Delta semblance analysis across Hanadir formation, the top left side is the depth migrated section with residual moveouts overlaid

Similarly, residual interval velocity analysis was created along the horizons to estimate the parameter (ε). (Figure 5.9). The result of this analysis indicate an inconsistent epsilon values as appears in the in the semblance section in the bottom left corner in Figure 5.9. However, at some residual moveouts locations along the Hanadir horizon, the values range from 0.10 to 0.40 with an average of 0.25. Likewise delta, the value is relatively close to what the result of the calculated parameter from the sonic well log. Although, the anisotropic parameters cannot be concluded from the seismic due to the fluctuations and the wide range of values, we could get a good approximation to the values. The parameters calculated from the well however were the ones used to update the velocity model.

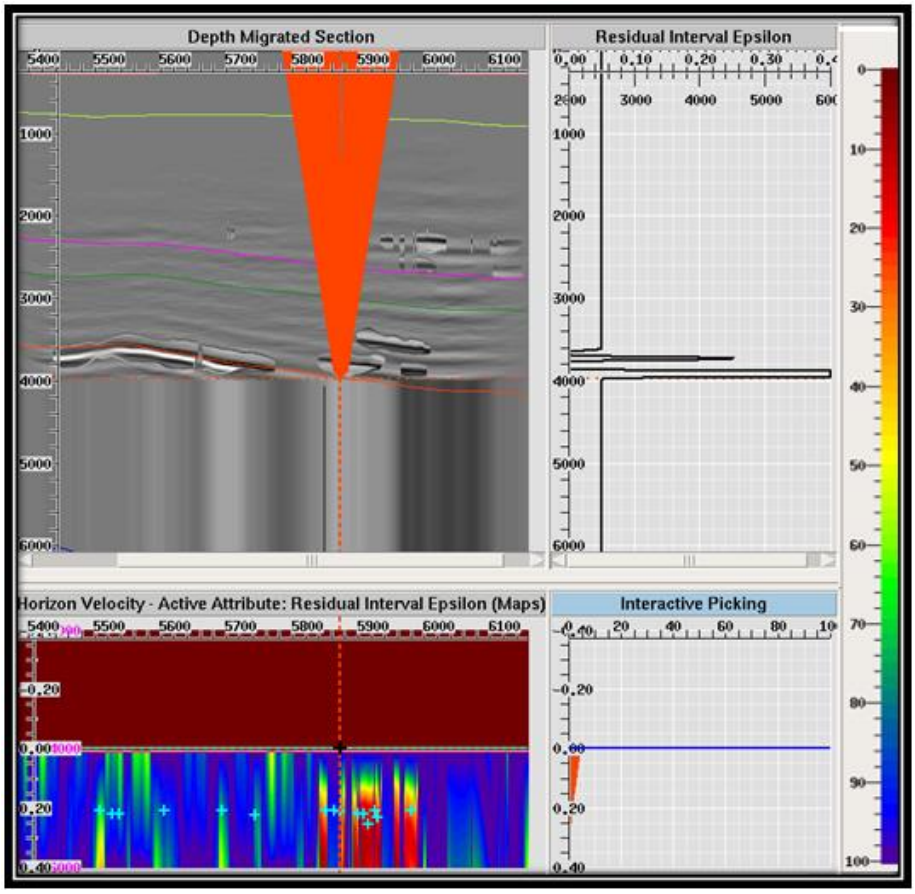

Figure 5.9. Residual analysis showing on bottom left corner interval Epsilon semblance analysis across Hanadir formation, the top left side is the depth migrated section with residual moveouts overlaid

The velocity model representation used in this work is a layer-based model where interval velocity information of each horizon is added to a set of interfaces. The Thomson parameters, ε and δ were also fed into the formation table, and a formation volume incorporating the anisotropic volume was created (Figure 5.10). Every color in the formation volume represent one formation. These formations are created based on the depth maps originated from converting the TWT maps to depth maps as discussed in Chapter 3. This formation volume was subsequently used to create two anisotropic volumes, delta and epsilon (Figures 5.11 and 5.12)

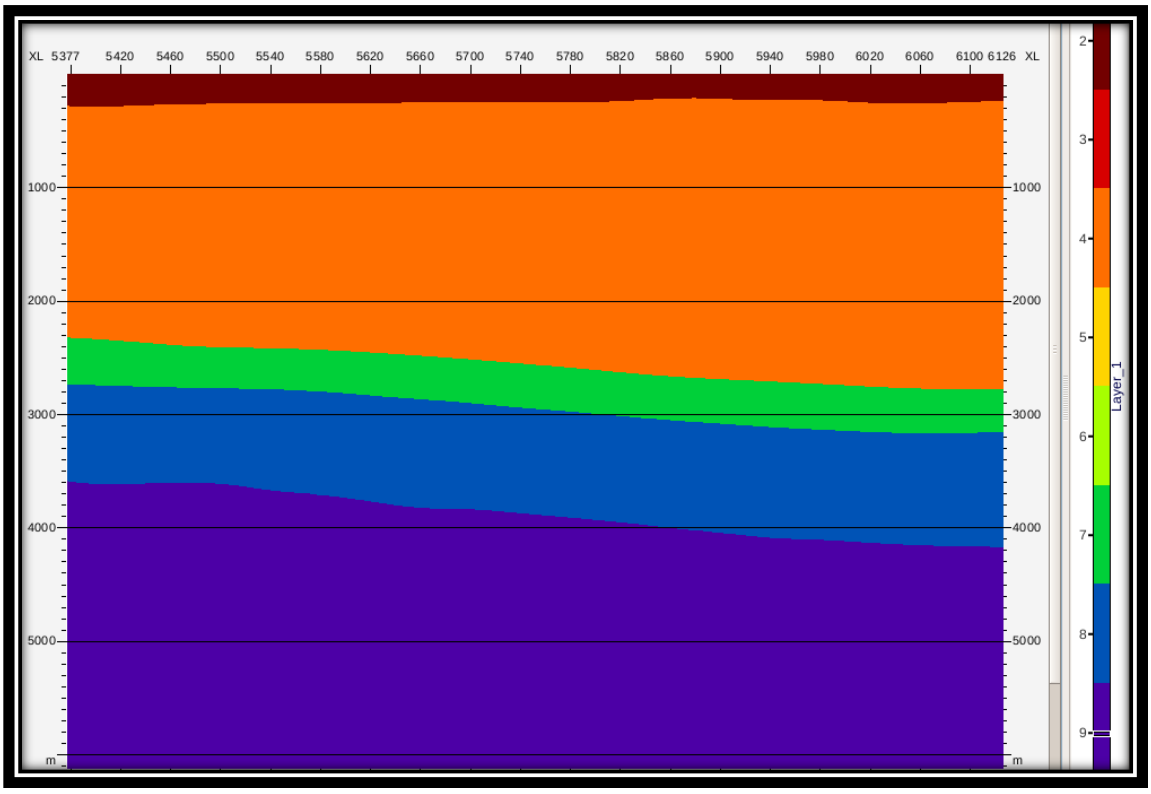

Figure 5.10. Formation volume for the Serri field project

At this stage, the anisotropic velocity model was created by updating the CVI model using the results from anisotropic parameters and residual moveout maps. Figures 5.13 and 5.14 show a 3D volume of the anisotropic velocity model and a cross section along IL1627.

The 3D Volume was our ultimate model for this study, although, more iterations of PreSDM can enhance the model when re-analyzing the residual moveouts. However, due to the expensive computation of PreSDM, this model will be sufficient to test the enhancement of the seismic record. The anisotropic velocity model incorporates the

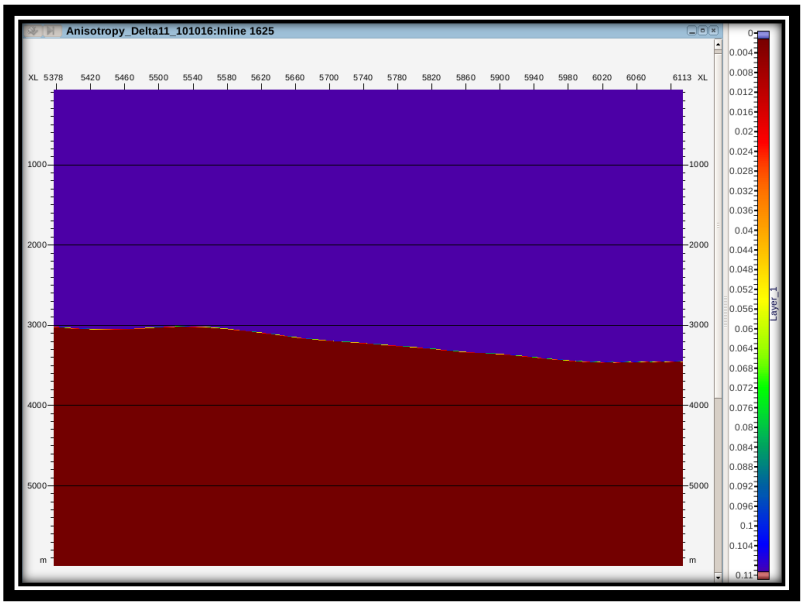

Figure 5.11 Interval delta cross-section at IL1625.

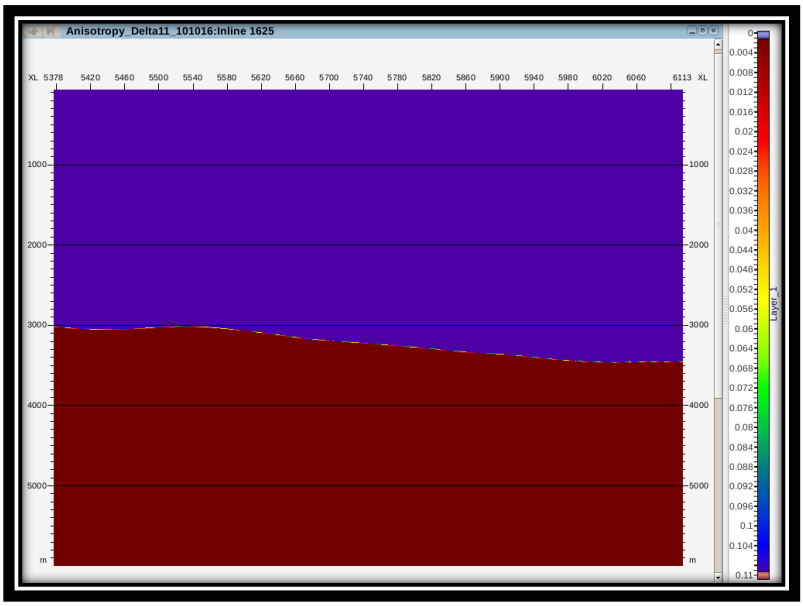

Figure 5.12 Interval epsilon cross-section at IL1625.

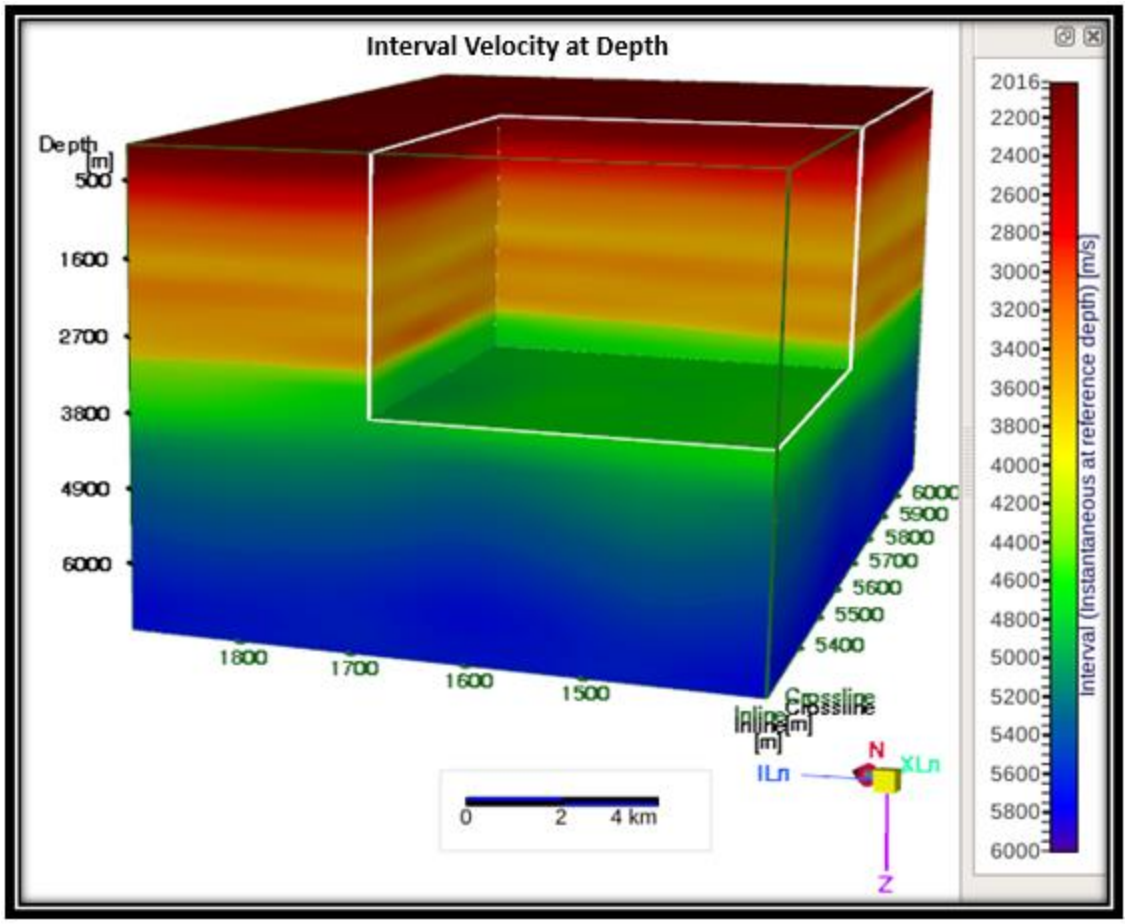

Figure 5.13. 3D volume of the anisotropic interval velocity in depth model.

intervals were determined. This velocity model was also smoothed in order to prepare it for our next iteration of PreSDM.

5.4 Anisotropic Kirchhoff Wavefront PreSDM

The anisotropic traveltimes are computed for each source and receiver pair by propagating wavefronts through the layered velocity model incorporating epsilon and delta parameters for each layer (Figure 4.1). Each time-increment points along a wavefront curve and is projected forward using an anisotropic ray velocity which is generally oblique to the wavefront direction. Once the anisotropic wavefront curves have been computed for each

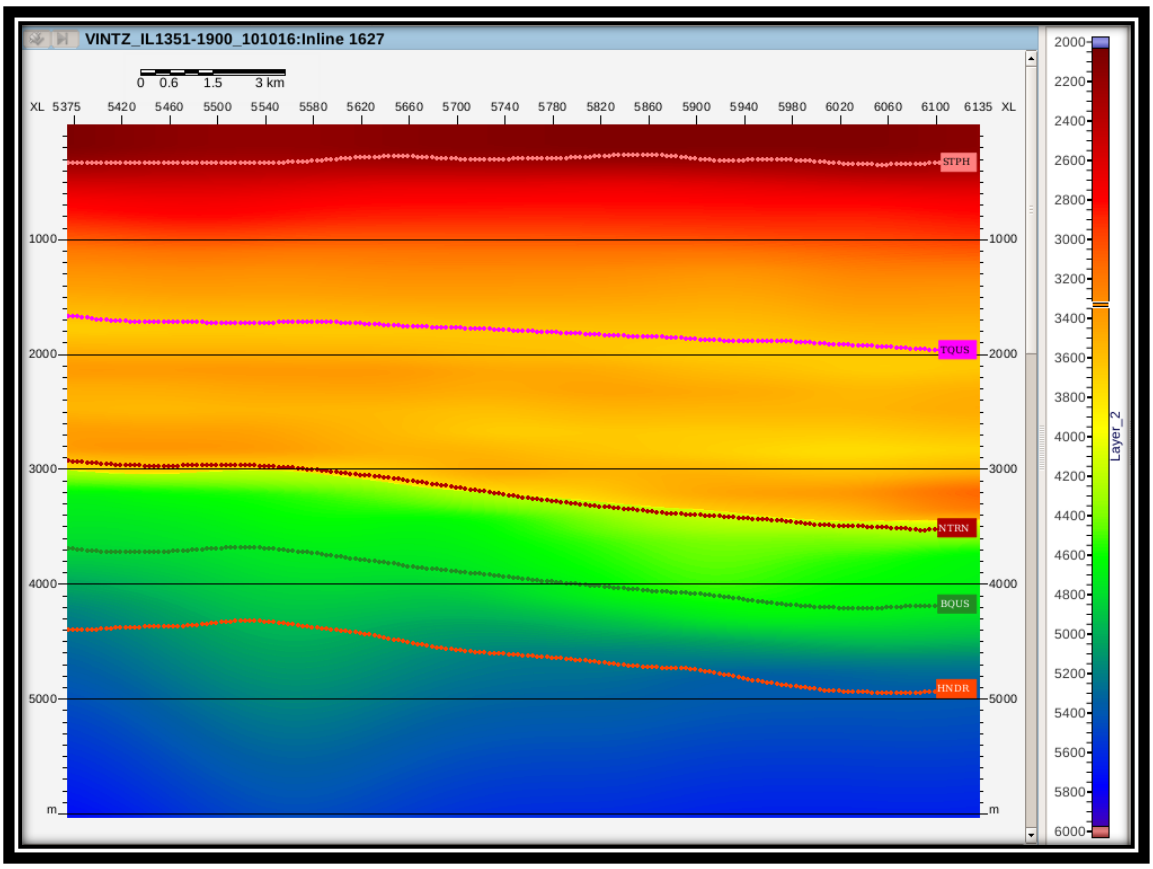

Figure 5.14. Anisotropic velocity section showing interval velocity at depth across IL1627. The lines are the TWT horizons converted to depth.

source and receiver pairs, a migration traveltime field for a given input trace is then calculated by adding the shot and receiver traveltimes for each point on the grid. Each input sample at time T is mapped to all depth locations (x, z) with the same traveltime (Vestrum, 1999).

The resultant depth gathers were then scaled back to time using the anisotropic velocity model. Figure 5.15 displays the gathers at the same locations of the isotropic example in Chapter 4. In this figure, we can see how the anisotropic velocity model did not only enhance the image quality but also corrected the moveout at the far offsets.

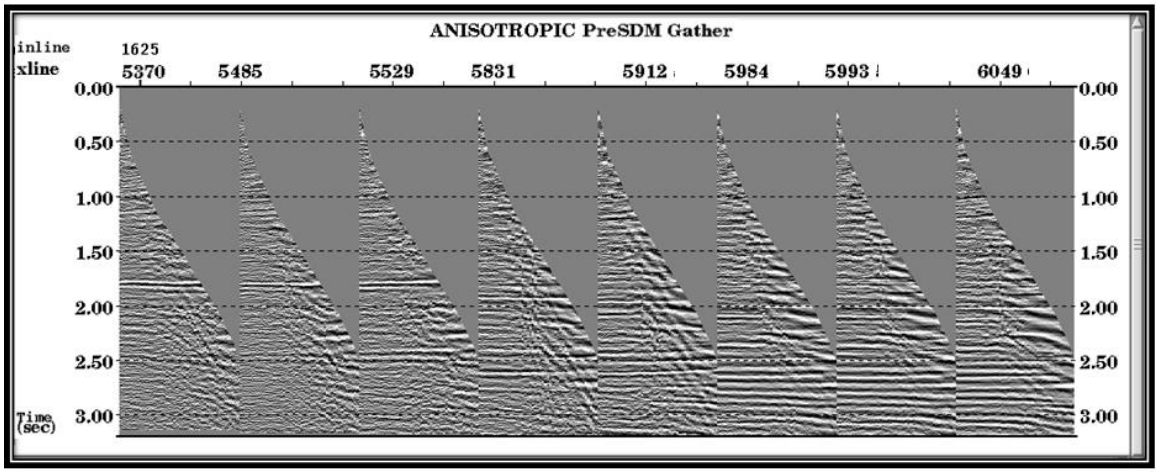

Figure 5.15. Multi-gather of anisotropic PreSDM gathers with 300 AGC.

Figures 5.16 and 5.17 are the anisotropic PreSDM stacks in both depth and time of IL1625 showing much improved reflections in comparison with isotropic stacks discussed in Chapter 4.

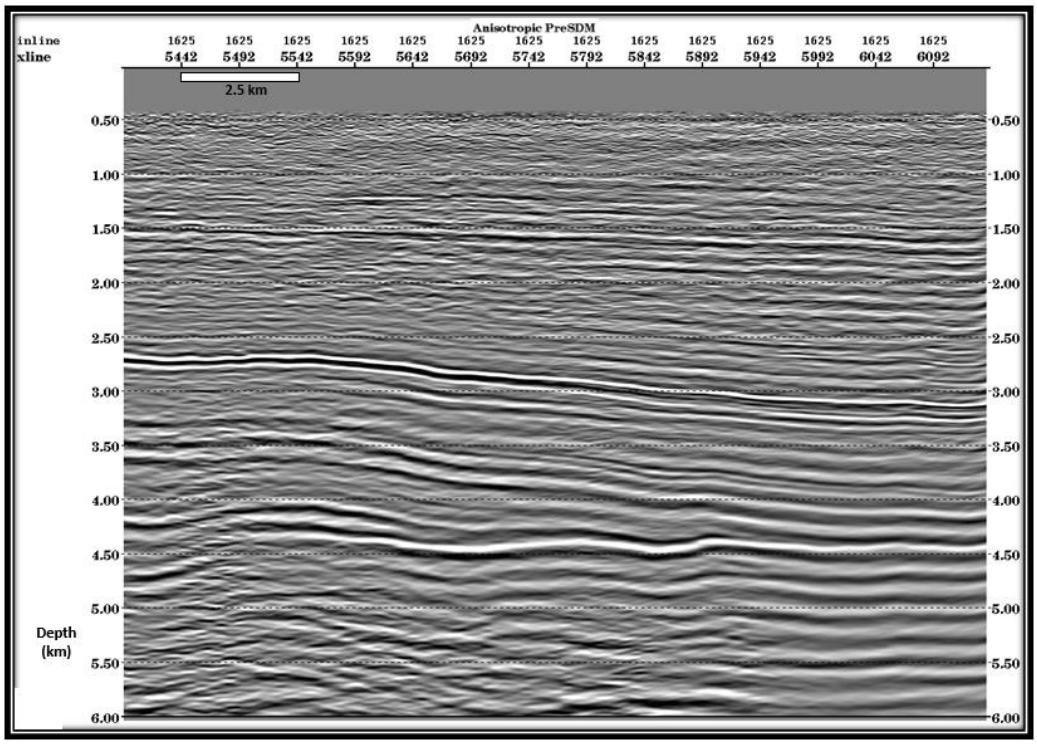

Figure 5.16. Seismic stack in depth from anisotropic PreSDM

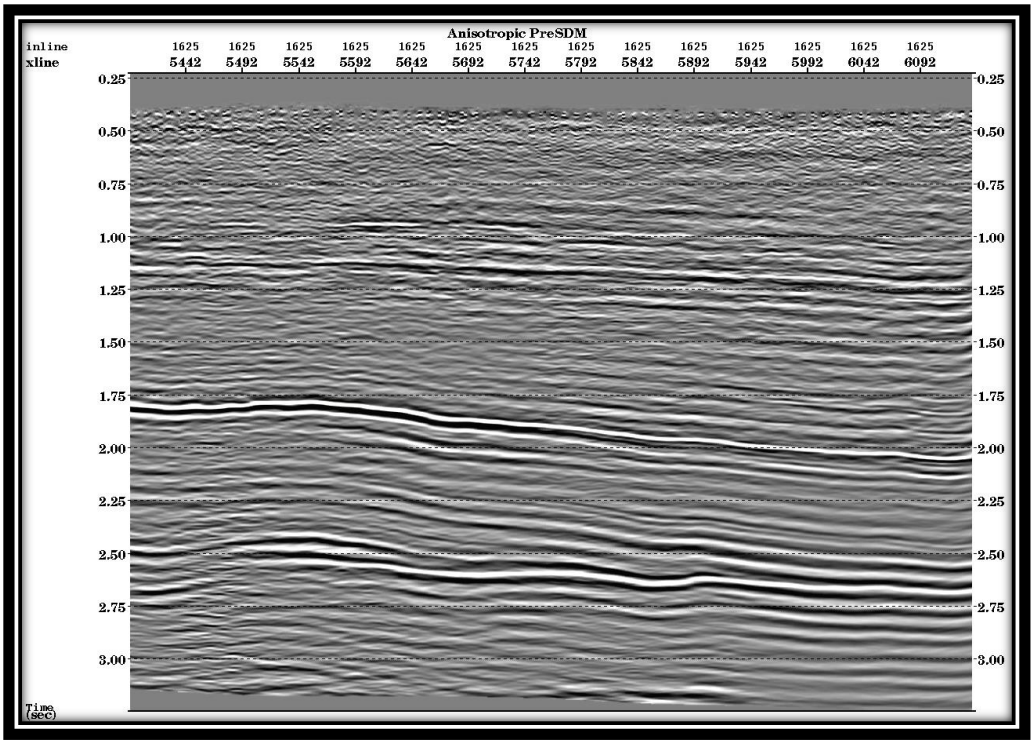

Figure 5.17. Seismic stack from anisotropic PreSDM converted to time.

Chapter 6

Isotropic Vs. Anisotropic PreSDM: Final Results and Discussion

The practical work to produce the final PreSDM results went through different velocity modelling stages. We firstly, ran an isotropic PreSDM using a geological constrained velocity model (CVI) which was subsequently updated to run a final PreSDM. The results throughout these stages were compared to check the improvement of the 3D seismic dataset.

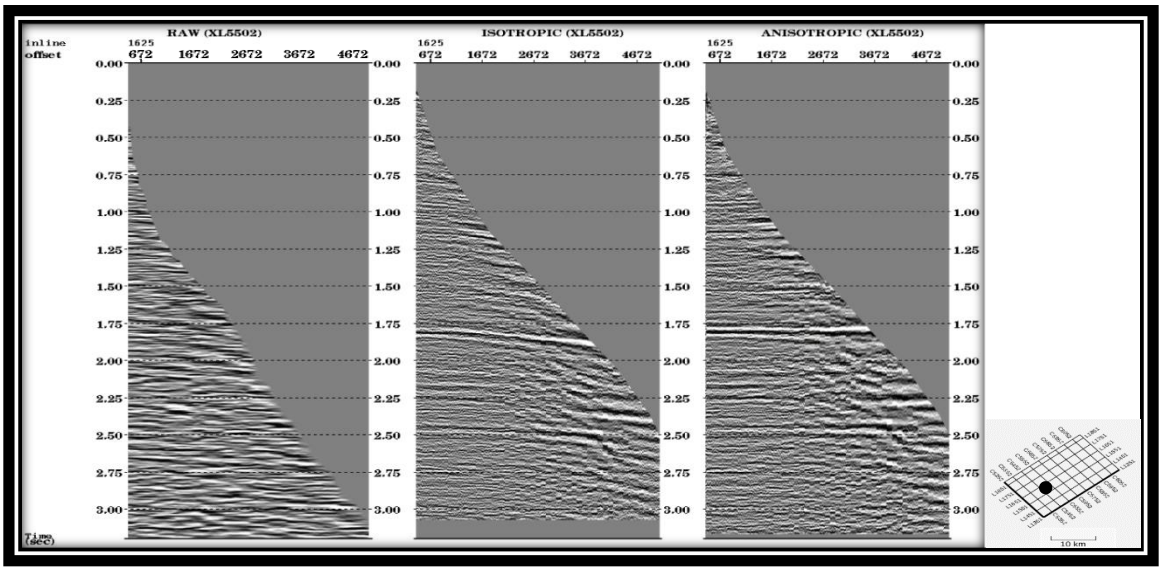

Figure 6.1 Comparison of CMP gather at XL5502 and IL1625, from left to right, (a) raw input, (b) after isotropic PreSDM, and (c) after anisotropic PreSDM.

Figure 6.1 shows a CMP gather comparison after two passes of PreSDM. From left to right: (a) the input CMP gather before migration, (b) is after isotropic PreSDM, and (c) is the after anisotropic PreSDM. We observe that the CMP gather in (a) is very noisy with reflections that can barely be noticed. TheCMP gather in (2) have reflections that are

consistently clear. However, we noticed that reflections in (b) are not flat at all offsets. After anisotropic PreSDM the CMP gather in (c) shows reflections that appear clear and flat laterally. This is most likely due the effect of the anisotropic parameters that were included in the velocity model used in the anisotropic PreSDM. Figure 6.2 compares the CMP gathers from different locations in the survey along IL 1625 where top (1) a collection of different CMP gathers after isotropic PreSDM, and bottom (2) is the CMP gathers after anisotropic PreSDM. In (1) we can notice the effect of seismic anisotropy at the far offset of the gathers throughout the seismic inline. Although isotropic PreSDM did a good job in making the reflections appear consistently better in (1) the reflections are not flat everywhere. The CMP gathers in (2) showed that the anisotropic velocity model helped to correct the behaviour of the reflections throughout the study area. Moreover, CMP gathers in (2) shows the deep reflections appear brighter and more defined.

Final seismic stacks were also compared from all the processing stages. Figure 6.3 shows from left to right (a) the CVS stack (input CMP gathers stacked with the initial stacking average velocity), (b) the stack from isotropic PreSDM gathers, and (c) the stack from anisotropic PreSDM gathers. It is clear that there is a progression of improved seismic imaging from left to right. The reflectors appear more robust and continuous throughout the section from left to right. It shows how effective the ray tracing migration method is in boosting up the energy. In addition, this imaging enhancement appears to be a result of performing depth migration, and in particular, using the structural interval velocity that took into account the lateral changes of velocity. Furthermore, the anisotropic stack does show a further improvement over the isotropic PreSDM stack.

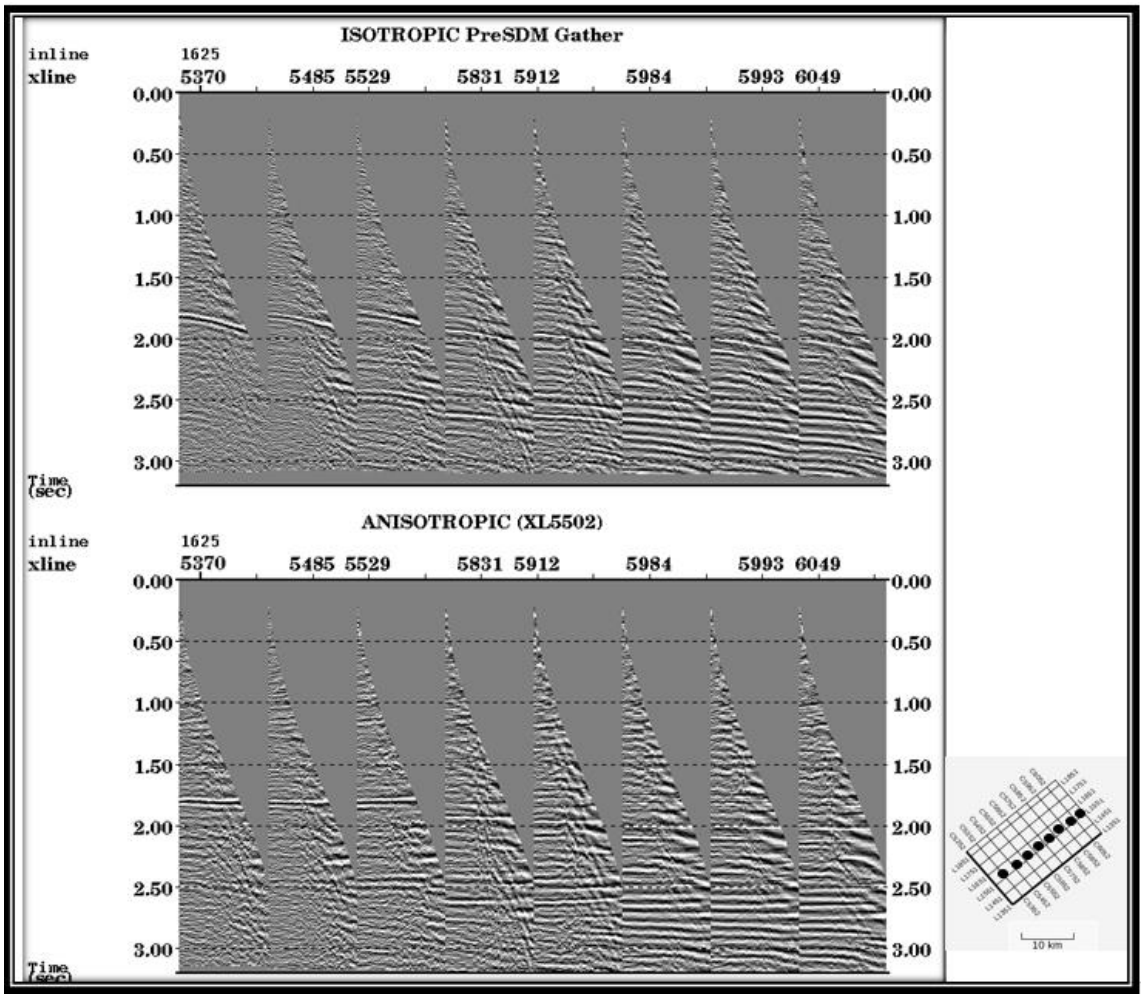

Figure 6.2. Comparison of top (1) isotropic and bottom (2) anisotropic PreSDM gathers.

In Figure 6.4, we compared the seismic stacks zoomed in at the event at the Base Qusaiba formation starting at 2.05 seconds, which is a formation where it sits on top of sandstone channels.(Saudi Stratigraphic Committee, 2013) The figure shows from top to bottom (a) CVS stack, (b) the stack after isotropic PreSDM, and (c) the stack after anisotropic PreSDM.The anisotropic result in (c) show that the PreSDM with the anisotropic velocity model has enhanced the overall imaging including the anticlines, and more importantly, made the reflections more continuous. Most likely anisotropic PreSDM move the events to their correct positions.

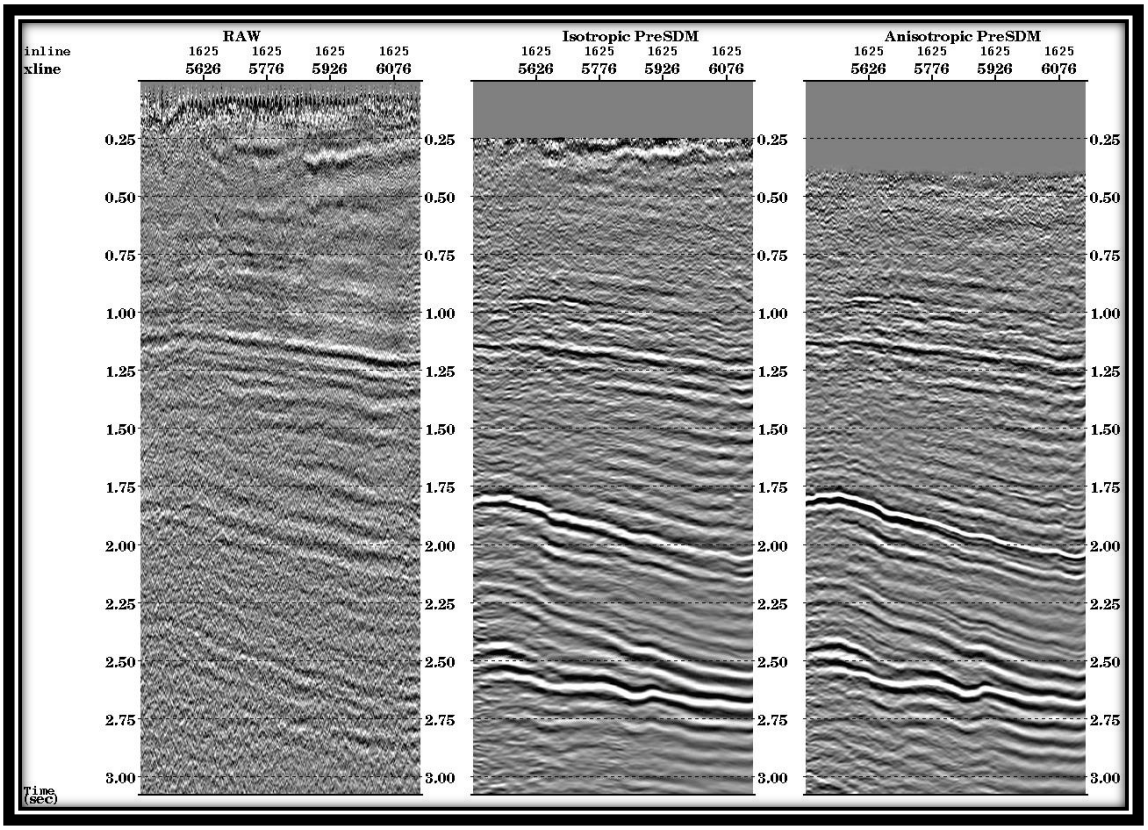

Figure 6.3 Seismic stacks comparisons: showing from left to right (a) CVS stack, (b) isotropic PreSDM stack, and (c) anisotropic PreSDM stack

Figure 6.5 show compares the stacks zoomed in across the Hanadir formation occurring at ~2.65 seconds. The figure from top to bottom shows (a) the CVS seismic stack, (b) isotropic PresDM stack, and (c) anisotropic PreSDM stack. The seismic event in stack (a) is barely visible, and therefore, not interpretable. The isotropic PreSDM gave a great improvement to boost up the event in (b). The Hanadir formation in (c) appears to be more continuous whereas it is artificially interrupted on (b) the isotropic stack.

Figure 6.6 is another stack seismic sections comparisons of the Serri field seismic data. The figure again compares the stacks, from left to right, (a) CVS stack, (b) isotropic PreSDM stack, and (c) anisotropic PreSDM stack. In this comparison, we noticed the

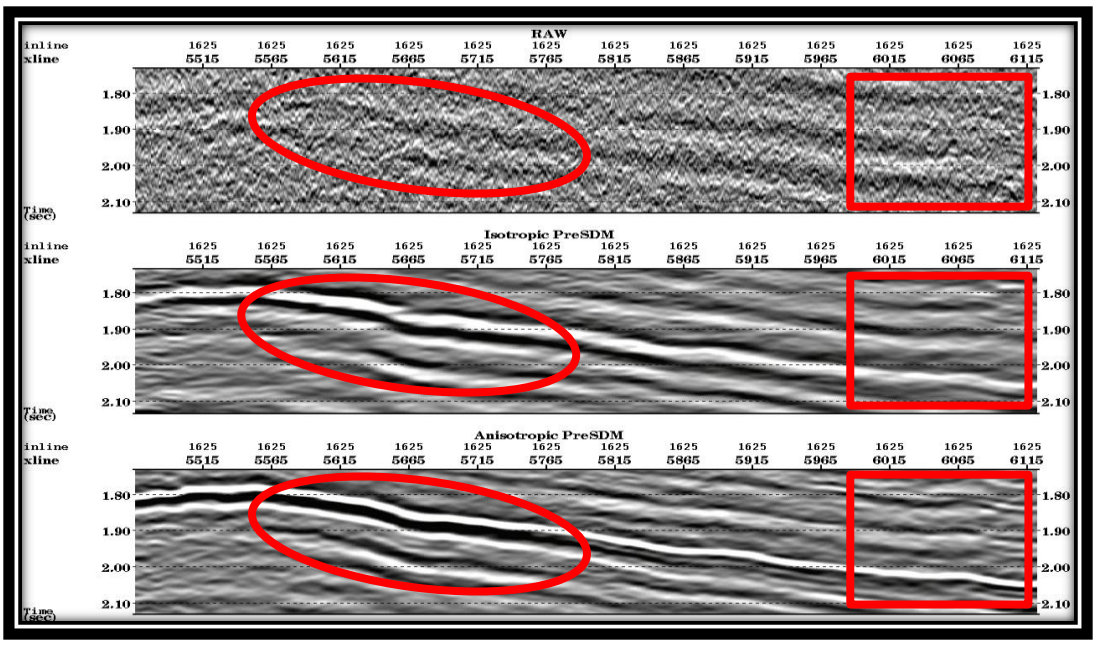

Figure 6.4 Seismic stacks comparisons, from top to bottom, (a) CVS stack, (b) isotropic PreSDM stack, (c) anisotropic PreSDM stack

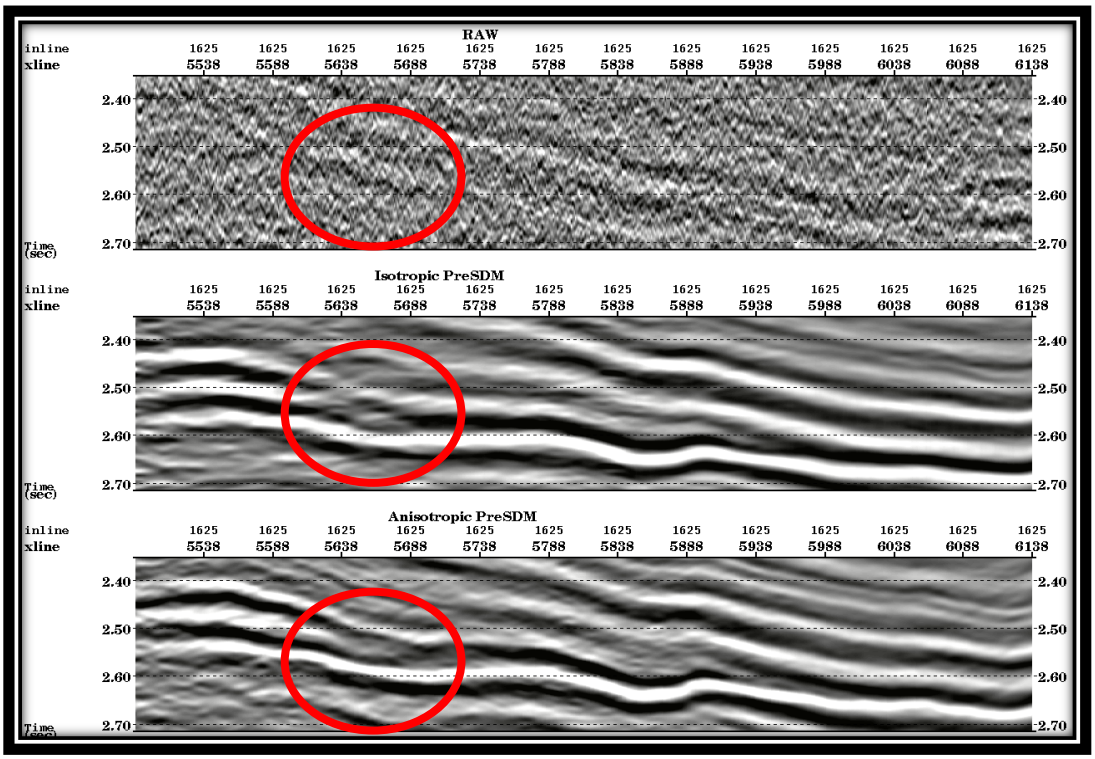

Figure 6.5. Seismic stacks comparisons: showing from top to bottom (a) CVS stack, (b) isotropic PreSDM stack, and (c) anisotropic PreSDM stack of Handir formation.

biggest improvement after anisotropic PreSDM. The event starting at 2.45 seconds highlighted in rectangle in (c) sharper and better focused than it is in the isotropic PreSDM in (b). This improvement is most likely because of the high degree of accuracy that the anisotropic velocity model has which consequently led to a better position of that event.

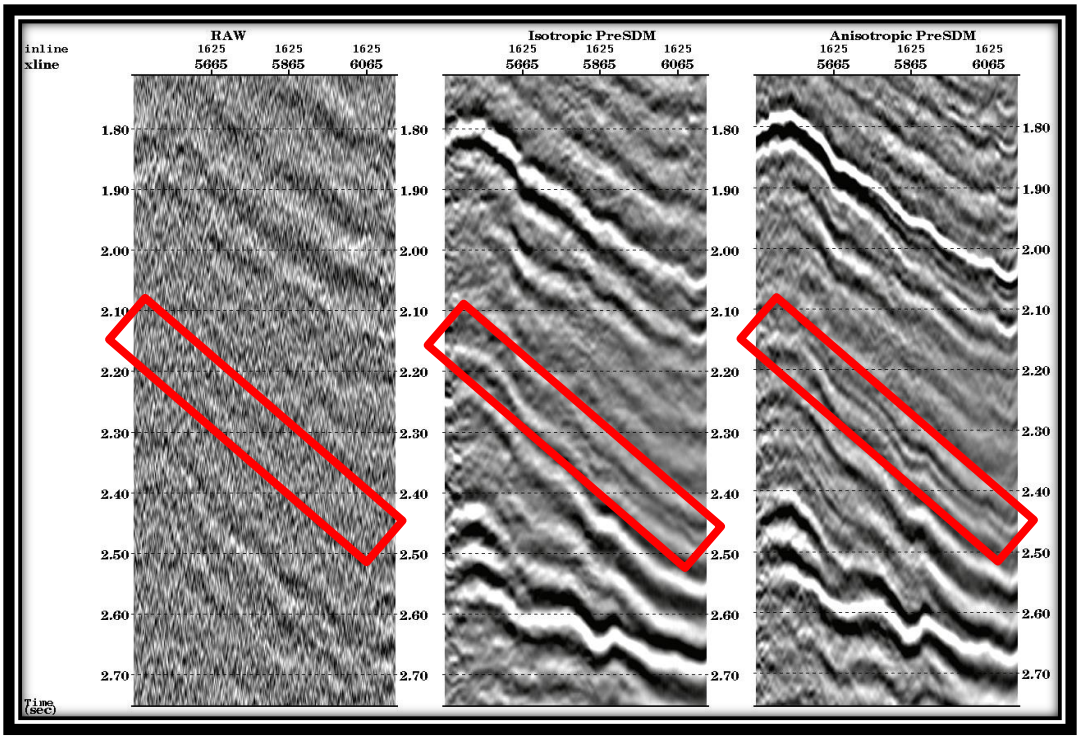

Figure 6.6.Seismic stacks comparisons: showing from left to right (a) CVS stack, (b) isotropic PreSDM stack, and (c) anisotropic PreSDM from 1.7-2.8 seconds.

Chapter 7

Conclusions and Future Work

7.1 Conclusions

Based on this study, three main approaches seem to make a significant impact on the improvement of seismic imaging of the subsurface: (1) elastic reflection coefficient characterizing heterogeneities present in the subsurface, (2) information on the variation of this reflection coefficient with incidence angle, and (3) information on the P-wave propagation velocity field in the Earth. A good detailed velocity model leads to a good seismic image. Velocity anisotropy is an essential information that must be accounted for in order to achieve the goal of accurately positioning the seismic events in a subsurface geology. It is because the presence of anisotropy causes two principal distortions in the reflection moveout: (1) incorrect vertical velocity will result in incorrect estimations of reflector depths, and (2) anisotropy leads to nonhyperbolic moveout which causes distortions in velocity estimation and deteriorates the image quality, if not corrected for (Helbig and Thomsen, 2005). The case study in this thesis demonstrated that seismic imaging whether isotropic PreSDM or anisotropic PreSDM is a powerful technique to boost up the energy in the seismic record and increase the S/N ratio. Anisotropic PreSDM in particular provides better focusing and more realistic subsurface reflections compared to isotropic PreSDM, and results in more accurate subsurface structures.

7.2 Limitation & Future work

The computation power has been the most persistent obstacle throughout the research. The workstation has a RAM of 32GB where best PreSDM results would require at least 48GB. Thus, the data was narrowed down to meet the available computation power. Another limitation was the extremely poor quality of the data. It has affected building up the initial velocity model. In other words, if the data had better acquisition parameters, a better S/N ratio would have been recorded, and thus, a better first run of velocity analysis would have been performed. Disk space was another issue. Although, 12 TB was thankfully provided, the raw shot gathers segy file has a size of 1.2 TB. The educational license of Paradigm Geodepth 15.0 did not include other algorithms for prestack depth migrations such Reverse Time Migration (RTM), and Common Reflection Angle Migration). If available, comparing the Kirchhoff's wavefront PreSDM to these algorithms would add more depth into the analysis of methods of seismic imaging. Moreover, it is thought-provoking to see update the anisotropic velocity model using horizon tomography and how it will reflect on the seismic imaging.

References

Alkhalifah, T. and I. Tsvankin (1995), Velocity analysis for transversely isotropic media, *Society of Exploration Geophysics*, 60,1550-1566.

Aruri K. R., P.J., Van Laer, M.H. Prudden, P.D. Jenden, W.J. Carrigan and A.A. Al-Hajji (2010), Controls on hydrocarbon properties in a Paleozoic petroleum system in Saudi Arabia: Exploration and development implications. *AAPG*, 10.1306/07060908133.

Anderson, B.I., T. Barber, R. Leveridge, and R. Bastia (2008), Triaxial induction – A new angle for an old measurement, *Oilfield Rev.* , 48-56.

Baptiste, Dale, S. Boyer, & K. Hellman (2015), True depth anisotropy in complex geological settings, *SBGF*, Rio De Janeiro.

Crampin, S. (1984), Evaluation of anisotropy by shear wave splitting: Applied Seismic Anisotropy: Theory, Background, and Field Studies, *Geophysics Reprint series*, 20, 23-33.

Dekel, G. (n.d), Anisotropy in Seismic Modeling and Imaging, *Paradigm Online University*. http://pdgm.com/online-university.

Harlan, W. (1999), Constrained Dix Inversion. http://billharlan.com/papers/rmsinv/rmsinv.html.

Helbig, K., L. Thomsen (2005), 75-plus years of anisotropy in exploration and reservoir seismics: A historical review of concepts and methods, *Geophysics*, VOL. 70, No. 6.

Ikelle, L.T. and L. Amundsen (2005), *Introduction to Petroleum Seismology, Investigations in Geophysics*, SEG Books, series No.12, Tulsa, Oklahoma.

Konert, G., A.M. Afifi, S.A. Al-Hajri and H.J. Droste (2001), Paleozoic stratigraphy and hydrocarbon habitat of the Arabian Plate, *GeoArabia*, v. 6, p. 407–442.

Koren, Z. and I. Ravve (2006), Constrained Dix inversion. *GEOPHYSICS*, 71(6), R113-R130.

Liu, Z. (1993), A Kirchhoff approach to seismic modeling and prestack depth migration. *62th Annual International Meeting, SEG Expanded Abstracts*, 888-891.

Mahmoud, M.D., D. Vaslet, and M.I. Al-Husseini (1992), The Lower Silurian Qalibah Formation of SaudiArabia: an important hydrocarbon source rock. *AAPG Bulletin*, vol. 76, n°10, October 1992, pp 1491-1506.

McBarnet, A. (2008), Why anisotropy can no longer be ignored. *Offshore Engineer*, http://offshore-engineer.com, April 2008.

McGillivray, J.G., and M.I. Husseini, (1992), The Paleozoic petroleum geology of Saudi Arabia, *American Association of Petroleum Geologists*, v. 76, p. 1473–1490.

Robein, E. (2010), Seismic Imaging: *A Review of the Techniques, their Principles, Merits and Limitations*. EAGE Publications, Houston, Texas.

Saudi Stratigraphic Committee. (2013), Phanerozoic Stratigraphy of Saudi Arabia Part 1 – Paelozoic succession of the Arabian Shelf. SGS-SP-2013-1

Stolt, R. and A. Weglein (2012), *Seismic Imaging and Inversion Application of Linear Inverse Theory*, Cambridge University Press, New York, New York

Thomsen, L. (2002), *Understanding seismic anisotropy in exploration and exploitation.* Society of Exploration Geophysicists, Tulsa, Oklahoma

Thomsen, L. (1986), Weak elastic anisotropy: Applied Seismic Anisotropy: Theory, Background, and Field Studies, *GEOPHYSICS*. VOL. 51. NO. 10, P. 1954-1966.

Toldi, J. L. (1985), Velocity analysis without picking. PhD thesis, Stanford University, Stanford, Californina.

Tsvankin, I. (1997), Anisotropic parameters and P-wave velocity for orthorhombic media, *Geophysics*, 62, 1292-1309.

Tsvankin, I. (2001), Seismic signatures and analysis of reflection data in anisotropic media: *Elsevier Science Publication*.

Upadhyay, S. K. (2004), *Seismic Reflection Processing*, Springer-Verlag. Berlin.

Vestrum, R. W., D.C. Lawton and R. S. Schmid (1999), Imaging structures below dipping TI media, *Geophysics*, 64, No. 4.

Wild, P. (2011), Practical applications of Seismic Anisotropy, *First break*, volume 29

Zeigler, M.A. (2001), Late Permian to Holocene paleofacies evolution of the Arabian Plate and its hydrocarbon occurrence, *GeoArabia*, v. 6, p. 445–504.